Structure and function of FNR1 from *Bacillus cereus* undergoing a mutation

In regard to electron transfer

Sondov Dahlen

Thesis for the master's degree in Molecular Biosciences
Main field of study in molecular biology and biochemistry
30 credits

Department of Biosciences
Faculty of Mathematics and Natural Science

UNIVERSITY OF OSLO

June 2021

2021

Structure and function of FNR1 from *Bacillus cereus* undergoing a mutation
Sondov Dahlen

http://www.duo.uio.no/

Trykk: Reprosentralen, Universitetet i Oslo

Acknowledgment

The work presented in this thesis was carried out at the Department of Biosciences, Faculty of Mathematics and Natural Science at the University of Oslo, from January 2021 to June 2021.

I would like to thank my supervisors Hans-Petter Hersleth and Marta Hammerstad for all the guidance both with laboratory work and writing this thesis. I feel very lucky to have ended up in your group and I am grateful for all the help you have given and how you have always been available.

I would also like to thank all my friends and fellow students at the university these past years, and especially Andreas Mikalsen, Jens Giskeødegård, Herman Graf and Anne Kristine Rugtveit.

Lastly, I would like to give a big thanks to my brother, Jardar Dahlen. Whenever the world seems crazy and life looks grim, it is good to have someone that shares your view of things.

Abstract

Ferredoxin/flavodoxin $NADP^+$ oxidoreductases (FNRs) are a group of enzymes assisting in electron transfer between $NADP^+$ and ferredoxins (FDs) / flavodoxins (Flds) by use of a flavin adenine dinucleotide (FAD). For *Bacillus cereus* three homologous FNRs (FNR1-3) exists but show large differences in the ability to reduce Flds. FNR1 is overall less efficient than especially FNR2, with values *for* k_{cat} being 10-100 times lower than FNR2. For FNR1 the C-terminal subdomain that stacks with the FAD cofactor has a conserved valine, where most other FNRs, including FNR2, has a histidine in this position. This difference is of interest as it might explain the contrast in electron transfer capacity. For this master project the goal was to mutate val329 in FNR1 to his329, in order to examine the difference this aromatic character makes.

During the project $FNR1_{mutant}$ was expressed and purified before crystallization and collection of diffraction data before solving the structure. Native-PAGE was run to examine the oligomerization state of $FNR1_{mutant}$. A series of experiments in anaerobic conditions were conducted to study the mutations effect on FNR's ability to reduce Flds.

After $FNR1_{mutant}$ was crystallized and structure solved, two different structures were revealed. The two structures had slight differences in conformation, with one structure being equal to $FNR1_{wild\ type}$ and one structure having a rotated NADPH-domain relative to the FAD domain. The structure of the $FNR1_{mutant}$ with rotated domains were further from the orientation in the structure of FNR2, and the mutation of valine to histidine did not change the structure to be more equal that of FNR2 with respect to the domain rotation.

Activity measurements were conducted in anaerobic conditions, examining k_{cat}, K_m and k_{cat} / K_m by use of UV-vis spectroscopy to measure concentrations and plotting reduction rates by use of the Michaelis-Menten function. During experiments $FNR1_{mutant}$ was shown to have slightly lower and k_{cat}, and similar or slightly higher K_m values. The mutation did overall decrease FNR1's ability to reduce Flds.

Content

1 Introduction

1.1 Background

This project has focused on the structure and function of ferredoxin/flavodoxin $NADP^+$ oxidoreductase 1 (FNR1) from *Bacillus cereus* regarding electron transfer and the effect of mutating valine329 to histidine329. These flavin-stacking residues are different in *B. cereus* FNR1 and FNR2, and hence, may play a role on the catalytic efficiencies of the FNRs. FNRs in *B. cereus* can reduce flavodoxins (Flds) by use of NADPH and the introduction section will cover the NADPH cycle, function of Flds and ferredoxins (FDs), electron transfer, structure of FNR1, mutation of FNR1, and the function of FNR1 compared to FNR2.

1.1.1 Flavins, flavoproteins, flavodoxins, and ferredoxins

Flavins are a family of versatile redox cofactors derived from riboflavin, commonly known as vitamin B2. Flavins have the ability to participate in both one-electron and two-electron transfers and play an integral role in electron transfer in biological systems [1] [2]. Flavoproteins are enzymes or proteins that have a flavin cofactor, with flavin adenine dinucleotide (FAD) and flavin mononucleotide (FMN) being the most common derivates of flavin (figure 1). FAD or FMN act as coenzymes when flavoproteins catalyze redox reactions [3].

The structures of FAD and FMN are characterized by a three-ring structure called isoalloxazine and it is this structure that is responsible for electron transfer. The isoalloxazine ring structure can be observed in different oxidation states, with oxidized, semiquinone, and hydroquinone forms being the most common. These different oxidation states can easily be observed due to differences in absorption spectra, with oxidized being yellow, semiquinone blue, and hydroquinone colorless (figure 2).

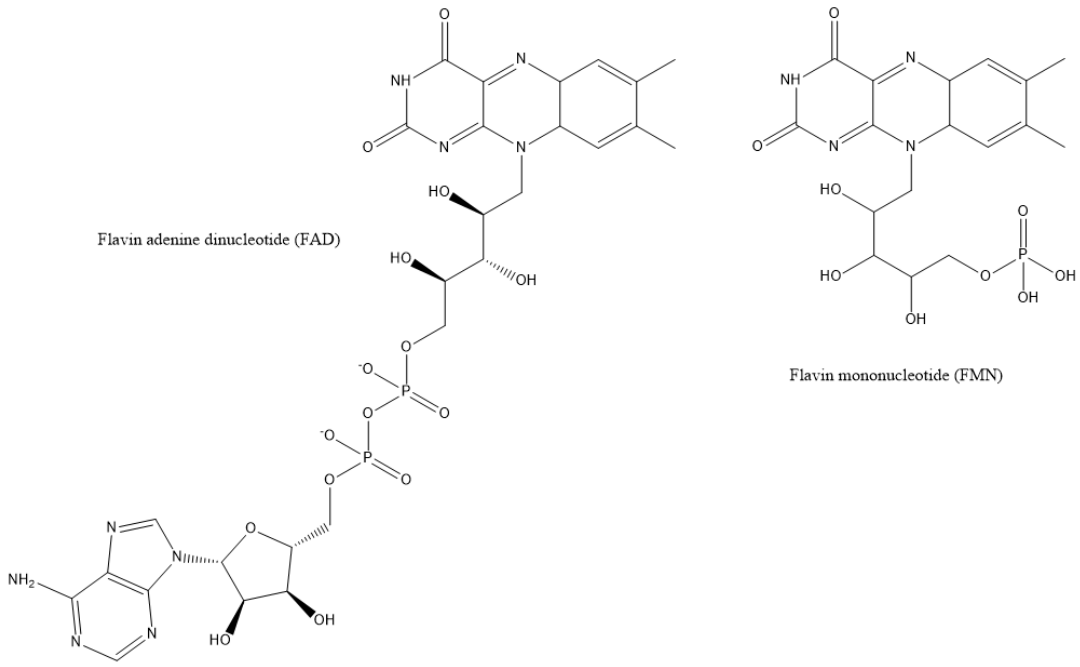

Figure 1 - Flavin adenine dinucleotide (FAD) and flavin mononucleotide (FMN) with the three ring isoalloxazine structure

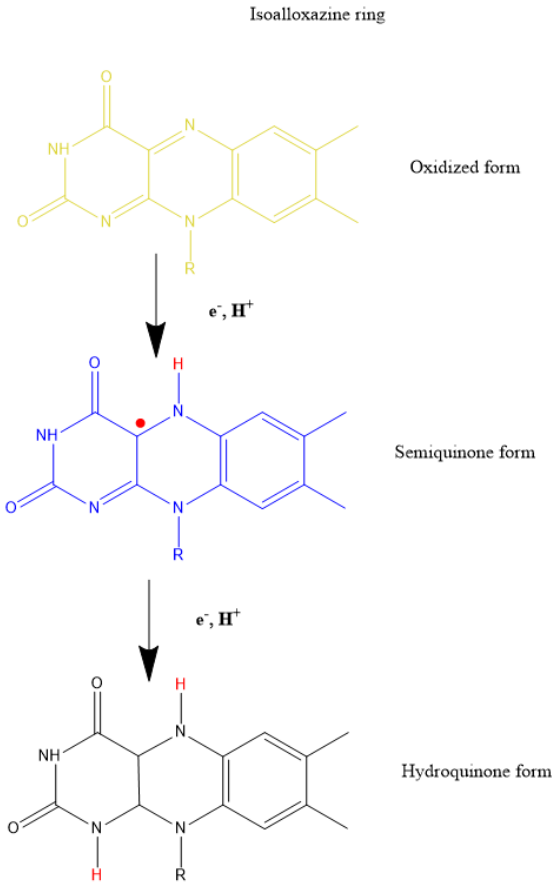

Figure 2 - Isoalloxazine ring in flavins at the three oxidation states. Oxidized (yellow), semiquinone (blue) and hydroquinone (colorless)

Flds are electron transfer proteins found in bacteria, containing an FMN as the prosthetic group [3]. The Fld structure is characterized by a Rossman-like fold consisting of five-stranded parallel β-sheet surrounded by α-helices [4]. FDs are iron-sulphur proteins that transfer electrons from one enzyme system to another. Both Flds and FDs serve a function in electron transfer together with FNRs [3] [5].

1.1.2 Ferredoxin/flavodoxin $NADP^+$ oxidoreductases (FNRs)

FNRs are a group of enzymes containing a FAD-group that assists in electron transfer between $NADP^+$ and FDs/Flds [3] [6]. FNRs occur as glutathione reductase (GR)-type FNRs and plant-type FNRs with further divisions. In this project, we have focused on the dimeric bacterial-type FNRs called thioredoxin reductase (TrxR)-like FNRs which are a subgroup of the GR-type FNRs. The binding site for NADPH in FNRs is in the three-layer sandwich with α/β/α Rossman-like topology domain for the plant-type FNR while FNRs from *B*. *cereus* use a β/β/α Rossman-like topology for both the NADPH and FAD binding domains [7]. In *B. cereus,* two Flds, an Fld-like protein, and two FDs exist and FNRs play a crucial role in reducing these. FNRs make use of FAD's ability to utilize an isoalloxazine ring as a coenzyme for redox reactions and FAD's can normally exist in three redox states as described above [8] [9]. FNRs can easily be distinguished by using the absorption and UV-spectrum from FAD where different oxidation states differ in absorption peaks and colors with oxidized form having a peak at 450-470 nm for FNR in *B. cereus* [10] [11].

1.1.3 Structure and function of FNR1

In *B. cereus,* there are three homologous FNRs (FNR1-3; BC0385, BC4926 and BC1495), and the focus of this project will be FNR1 [12]. The NADPH-binding domain and the FAD-binding domain are connected by a short hinge consisting of an antiparallel β-sheet (figure 3). Experiments where glycine residues in the hinge region, gly260 and gly266, were replaced with proline residue showed a drop in catalytic activity for FNR, indicating the importance of the hinge region. The lack of interactions between the domains makes rotation easy and this hinge region makes two reduction steps possible as the NADPH-binding site is suggested to rotate once FAD is reduced, enabling an additional reduction [6] [13] [14].

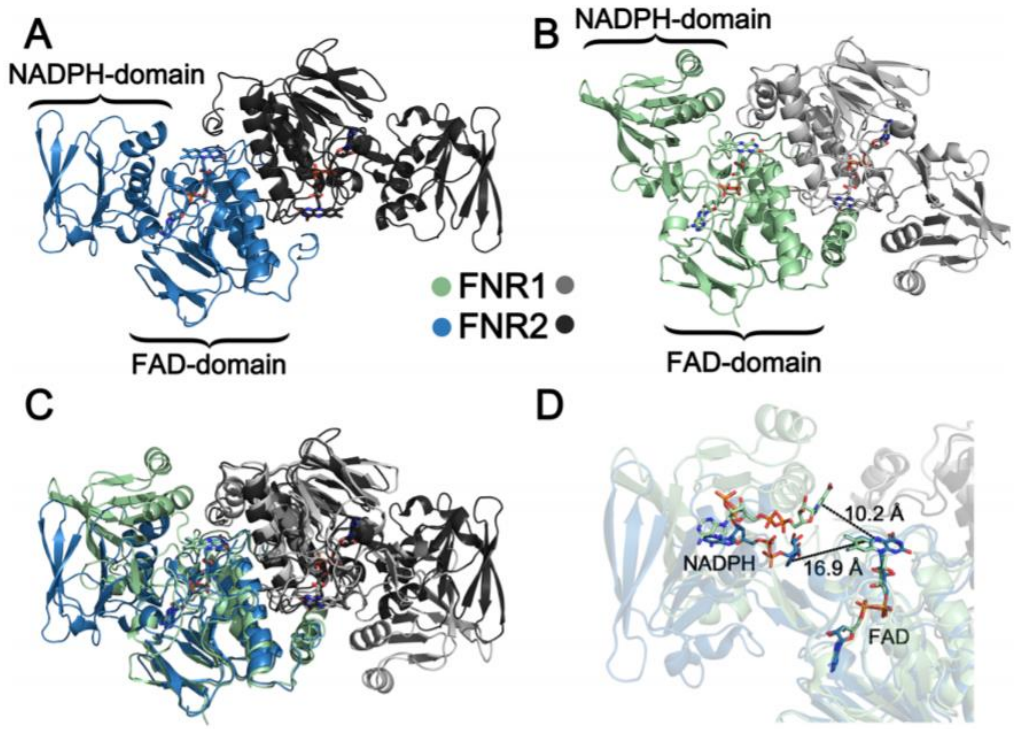

Figure 3 – Crystal structure of the dimeric B. cereus FNR2 shown in blue and black (A). B. cereus FNR1 shown in green and grey (B), with NADPH-domains and FAD-domains indicated by brackets. Overlay of structures (C) and distance between NADPH-binding site and the FAD cofactor in FNR1 and FNR2 (D)). Figure from [6]

Structures of FNRs in *B. cereus* and *Bacillus subtilis* have shown NADPH binds too far away from FAD to allow hydride transfers in these structures. The crystal structure of FNR1 from *B. cereus* has a more closed conformation with respect to the Fld binding site and with NADPH positioned 10.2 Å away from FAD (figure 3D) [6]. While electron tunneling can take place at distances up to 14 Å, hydride transfers are expected to occur at distances of 1-2 Å. This indicates that a large-scale conformational rearrangement is required for efficient functionality [6] [15].

B. cereus FNR2 in comparison, has a more open conformation and binds NADPH 16.9 Å away from FAD and can more easily fit a Fld substrate for electron transfer (figure 3D). FNR1 on the other hand most likely requires conformation changes to allow substrate binding[16]. FNR1 and FNR2 also show significant differences in amino acid sequence in the surface region for binding substrates. FNR1 has small patches of basic pH residues on several places of the surface, while FNR2 has a single large patch around its FAD cofactor. When modelling binding of the Fld substrate, the FNR1 FAD cofactor is accessible, but the basic patch is smaller than in FNR2. This is another feature which can influence electron transfer [6].

Another way FNR1 differentiates from other TrxR-like FNRs is on the C-terminal subdomain that stacks above the FAD cofactor. Here, most other FNRs have a residue with aromatic character followed by two aliphatic hydroxyl-containing residues, which have been found to stabilize the FAD cofactor. In FNR1, this aromatic residue is replaced by a valine, and is conserved in FNRs in several bacteria [6].

1.1.4 The ribonucleotide reductase system

DNA synthesis is crucial for all living organisms, for this to happen the supply of deoxyribonucleotide triphosphates (dNTPs) or deoxyribonucleotide diphosphates (dNDPs) is crucial. The only biochemical pathway for de novo synthesis of deoxyribonucleotides is catalytic reaction with ribonucleotide reductase (RNR) [17]. RNR are classified into three different groups: I, II and III, with further subdivisions of class I RNRs into classes Ia, Ib, Ic, Id, Ie[18]. Class I RNRs are characterized by two subunits, the catalytic α_2 subunit and the radical initiating β_2 subunit. In order to reduce ribonucleotides to their corresponding deoxyribonucleotides, a cysteinyl radical ($S^{\bullet}$) in the catalytic site of the α_2 subunit of RNR is used. In subclasses Ia and Ib, this $S^{\bullet}$ is generated by a metallocofactor in the β_2-subunit, an $Fe^{III}Fe^{III}$-tyrosyl radical (Y•) cofactor in class Ia, and a $Mn^{III}Mn^{III}$-Y• cofactor in class Ib. In the bacterial class Ib RNR the activation of this metallo-cofactor in class Ib requires the Fld-like protein NrdI. NrdI works by first reducing a dioxygen to superoxide, which then oxidizes the metal cluster, and hence, generates the Y• [19]. RNR activity is controlled indirectly by the efficiency of FNRs to reduce NrdI, and hence, FNRs play a crucial role in the pathway of DNA synthesis in class Ib RNR.

1.2 Electron transfer and enzymatic activity

Flds play an integral role in transferring electrons to various redox enzymes, and for this to happen the Flds must first be reduced by FNRs. Several FNRs have been shown to be able to reduce Flds, but the enzymatic activity and speed of electron transfer varies [6].

1.2.1 Electron transfer of the FNR family

The three homologous FNRs (FNR1-3) in *B. cereus* have all been tested for binding with NrdI, Fld1, and Fld2. Experiments show all FNRs bind to NrdI and Flds, but at slight variations in binding efficiency. Furthermore, UV-visible spectroscopy in anaerobic conditions has been used to see if FNRs can reduce NrdI and Flds. Here, the differences between the FNRs are larger, with FNR2 being much higher turnover than its FNR1 and FNR3 counterparts (table 1) [19].

Table 1 – Kinetic parameters for reduction of NrdI and Fld2 by different FNRs from B. cereus. Data from [6]

FNR1			
	k_{cat} (min^{-1})	K_m (μM)	k_{cat} / K_m (μM^{-1} min^{-1})
NrdI	8.0 ± 0.1	2.7 ± 0.2	3.0 ± 0.4
Fld2	42 ± 8	60 ± 22	0.7 ± 0.4
FNR2			
	k_{cat} (min^{-1})	K_m (μM)	k_{cat} / K_m (μM^{-1} min^{-1})
NrdI	100 ± 4	61 ± 5	1.6 ± 0.2
Fld2	9125 ± 1450	13 ± 5	701 ± 360
FNR3			
	k_{cat} (min^{-1})	K_m (μM)	k_{cat} / K_m (μM^{-1} min^{-1})
NrdI	2.94 ± 0.04	0.74 ± 0.06	3.9 ± 0.4
Fld2	2.9 ± 0.3	8 ± 2	0.4 ± 0.2

1.2.2 Comparing FNR1 to FNR2 in structure and function

While all FNRs can reduce NrdI and Flds, it is clearly shown that FNR2 is by far the superior choice. Why this is and what differences between the FNRs would be interesting to find out. In this project the focus will be to investigate FNR1 and comparing the structure of the more efficient FNR2.

FNR1 and FNR2 differ in open vs closed conformation, how far away NADPH binds from FAD, difference in amino acid sequence in hinge regions, and the basic patches on the surface for binding substrate. Lastly the FNR1 C-terminal subdomain that stacks with the FAD cofactor differs by having a valine where the majority of TrxR-

like FNRs have residues with aromatic characters [6]. This domain is close to the FAD binding site, stacking with the isoalloxazine ring structure and the aromatic residue might play a role in the efficient reduction of NrdI and Flds.

1.3. Aims of the master project

The focus of this project is FNR1 from *B. cereus* and its structure and function. FNR1 has shown to be able to reduce Flds and NrdI, but at a lesser rate than *B. cereus* FNR2, and have structural characteristics that differs from other FNRs. Especially the structural differences in the C-terminal subdomain, earlier found to be stabilizing for the FAD cofactor is of interest. In the binding site for FAD, FNR1 has a conserved valine where all other TrxR-like FNRs have a histidine. The goal is to gain knowledge of the effect made by the aromatic residue stacking with the FAD cofactor, how it affects the structure, and comparing the rate of electron transfer.

To complete this goal FNR1 must undergo a mutation of val329 to his329 before expression of protein and purification. To determine how the aromatic character affects the structure, FNR1 must be crystallized and the structure solved. To investigate the rate of electron transfers, kinetic studies will be performed, comparing $FNR1_{mutant}$ to $FNR1_{wild\ type}$ and $FNR2_{wild\ type}$.

Mutation of val329 to his329

To investigate the structure of FNR1 in comparison with FNR2 a single point mutation of val329 to his329 in FNR1 in *B. cereus* must be enacted. This will be performed by using a commercially ordered vector with the desired gene. FNR2 has a histidine in this spot, and the aromatic ring stacks with the flavin plane. This might play a role in stabilizing and increasing efficiency of FNR2. Mutating FNR1 and giving it the aromatic characteristic can indicate whether this plays a role.

Protein expression and purification

The first subgoal of this project is expression of $FNR1_{mutant}$ and purification. Wildtype FNR1 that will be used for comparison is available from previous studies on FNR1. After single point mutation of FNR1 has been completed, competent *Escherichia coli*

cells will be transformed and the $FNR1_{mutant}$ will be overexpressed, before purification by ion exchange chromatography and size exclusion chromatography.

Crystallization and structure

To examine the structure of $FNR1_{mutant}$ the second subgoal is to crystallize and collect X-ray diffraction data. After collecting diffraction data, the structure will be solved, and the structure interpreted in view of the main goal.

Electron transfer

To compare the effect of the mutation FNR1 will undergo steady-state reduction experiments in anaerobic conditions. The enzyme activity for FNR1 paired with NrdI and Fld2 will be measured, and the activity of $FNR1_{mutant}$ compared to $FNR1_{wild\ type}$.

2 Methods

2.1 Bacterial transformation

Principle

Transformation is the genetic alteration of a cell where a bacterium takes up foreign genetic material. When making synthetic alterations a vector with the desired mutations is usually necessary. This vector can be a plasmid compatible with the host cell, where restriction enzymes can cut sequences in both the vector and the bacteria, making insertion possible. To first get the vector inside the cell, the cells need to be competent. This can be done by keeping the cells cold in the presence of calcium phosphate to make the cell permeable and after using a heat shock treatment to cause the DNA vector to enter the cell [20].

After insertion of vector into bacterial cell the samples must be left to grow in the presence of a growth medium. After initial growth the samples are plated on agar plates. Plasmid and bacterial cells are usually made in a way that antibiotics can be used as a control, where non-transformed cells would die. The only bacteria colonies present on agar plates should be those who have successfully transformed and have antibiotic resistance. A single colony can be selected from the plates for further growth. This colony is multiplied by growth in the presence of a medium, and as a control step a sample is taken out where synthesis of the desired protein is induced. After inducing protein synthesis, the presence of desired protein is checked by use of sodium dodecyl sulphate–polyacrylamide gel electrophoresis (SDS-PAGE) where the size of protein is used as an indicator. If the control is successful the sample of transformed bacteria can be frozen for later use, where glycerol is used to prevent the formation of ice crystals [21].

Procedure

Plasmids containing the desired genes were ordered from GenScript (See Appendix). For transformation a pET-22b (+) vector with the desired mutation of valine329 to histidine329 was used. Vials with plasmid were centrifuged at 6000 x g for 1 minute at 4 ºC. Plasmids were dissolved in distilled water to a concentration of 50 ng/µl and vials vortexed for 1 minute. One Shot™ BL21(DE3) chemically competent *E. coli* cells

(Novagen) were thawed on ice and stirred carefully before transferring 10 µl cells to PCR-tubes while keeping it on ice.

Transformation was done with three different plasmid concentrations: 50 ng, 100 ng, 150 ng as well as one sample with 50 ng control plasmid (pUC 19) and one sample without plasmid. After adding plasmid to the competent cells, the transformation reactions were incubated on ice for 5 minutes, before heat shock at 45 ºC for 45 seconds. The reactions were then put on ice for 120 seconds before adding 125 µl Lysogenic Broth medium (LB-medium) to each tube. The reactions were incubated at 37 ºC for one hour at 250 rpm. After incubation, reactions were spread on agar plates containing 100 µg/ml ampicillin, where both high and low sample volume was tested. Plates were wrapped in parafilm and incubated overnight at 37 ºC

Bacteria colonies from agar plates was inserted into tubes with 5 ml LB medium (see appendix) and 100 µg/ml ampicillin, 2 colonies from each plate. Incubation overnight at 37 ºC and 250 rpm. Next day samples were taken out, with 100 µl culture for 5 ml LB and 100 µg/ml ampicillin and let grow for 2 hours before inducing protein expression with IPTG to a concentration of 5 mM at OD_{600nm} 0.8 for each tube. After induction a bacterial pellet was made by centrifugation. A sample of Pellet was diluted with 37.5 µl water and 12.5 µl loading dye before test on SDS-PAGE for protein expression. After presence of FNR1 was confirmed, glycerol stocks were made (glycerol concentration of 12%), and the samples were frozen in liquid nitrogen and stored at -80 ºC.

2.2 Bacterial growth conditions

Principle

For growth of transformed bacteria, a series of conditions are set for optimal growth as described below. A LB-medium is used for normal growth and provides a nutrient rich environment with added ampicillin to prevent non-transformed bacteria from growing. In addition to the use of ampicillin to prevent other bacteria from growing, an autoclave is used to sterilize containers and equipment. Growth for LB medium is done at 37 ºC which is the preferred temperature for *E. coli* and most other bacteria, and pH is kept neutral. A shaker is necessary for proper growth.

After initial growth a sample is taken out and then transferred to a new batch of LB medium, this to ensure more equal bacterial growth conditions making reproduction possible, as well as making sure the bacterial growth is in the proper phase, with either stationary phase or logarithmic growth phase. Not switching medium risks that the bacteria are in a stationary or death phase as the nutrition is being used up or toxic byproducts are made.

When changing to large scale growth, terrific broth (TB) medium is used instead, as it is more nutrient rich. Growth is measured by use of optical spectroscopy and measured at OD_{600nm}. Values at ~ 0.7 OD indicates the bacterial growth is inside to logarithmic phase. During this phase IPTG is added, which induces production of desired protein. Adding IPTG during log phase provides optimal balance between bacterial growth and protein synthesis. A lower temperature can at times be used to reduce growth rate and can benefit proper protein synthesis and folding.

Procedure

For overexpression of protein, a sample was selected from freezer and a tiny amount added to 10 ml LB medium with 100 µg/ml ampicillin. Bacteria grew overnight for approximately 16-18 hours at 37 ºC. Following day 5 ml sample was taken out and added to 100 ml LB medium with 100 µg/ml ampicillin before growing for 6 hours at 37 ºC. A final dilution with 10 ml culture was added to TB medium with 100 µg/ml ampicillin for 1L TB medium. Bacterial cultures were left to grow at 30 ºC until OD_{600nm} 0.6-0.8 before putting samples on ice and adding 1 mM IPTG. After inducing temperature is reduced to 18 ºC and left until next day. All bacteria growth is done at 250 rpm.

2.3 Extraction and purification of protein

Principle

For extraction of protein it is necessary to break up bacterial cell walls and separate protein from cell-debris. While extracting protein it is important to ensure protein remains intact, and several additives such as stabilizing agents and protease inhibitors can be used, as well as keeping sample on ice to reduce activity. For breaking up cell walls and extracting proteins a few methods can be used, such as

French press, sonication, high temperature or chemical additives. After breaking up cell walls the next goal is to separate protein from cell-debris. Large particles such as the DNA backbone needs to be broken down in manageable sizes by use of enzymes before separation. Separation of protein can be done by using the different solubility of protein and cell-debris. Salt increases the ionic strength and reduce the solubility of proteins. Ammonium sulfate is often used for this and by increasing salt in solution solubility is decreased and separating can be done based on salt concentration.

Prior to purification the first step is desalting the protein by use of size exclusion chromatography, to remove ammonium sulfate and other ions that may be in solution. Salts and other molecules from extraction may have adverse effects on protein stability or function and should be removed before further purification. Desalting is done by use of a size exclusion column which use a porous resin where molecules of smaller size use longer time to traverse the distance as they enter the pores and slowing the rate of migration. There is a large difference in size between the protein and the salt, and this cause the salt to use longer time to traverse the column. To control what fractions have the desired protein light absorption at 280 nm can be used as proteins in general absorb light at this wavelength [22].

After desalting purification is done by ion exchange chromatography. Ion exchange use the principle of pH affecting the charge of the protein and either a cation or anion column. The charged proteins in solution will bind to the column while particles with insufficient charge will elute. A buffer with high salt concentration is used to gradually decrease binding to column. While increasing salt concentration particles with high charge density will elute later, while particles with lower charge density such as proteins emerge first [23]. By using light absorption at 280 nm and 450 nm fractions can be controlled to see when proteins emerge.

The final purification step is performed by gel filtration (GF) (size exclusion chromatography). Ion exchange chromatography can remove particles that differs in charge, while size exclusion chromatography will remove other particles that have equal charge but differs in size, such as other proteins in solution.

Procedure

After overnight growth of bacteria in TB-medium pellets are made by centrifugation at 5 000 g for 10 minutes. Bacterial growth was done in 2 operations of 4 L TB-medium each time. Supernatant was removed and pellet dissolved by use of lysis buffer (See appendix) in a 1:4 ratio of cell wet weight to lysis buffer. Cells were lysed by sonication at 60ml batches at 50% amplitude, with 3 bursts of 20 sec followed by intervals of 40 sec cooling on ice. Particulate matter was removed by centrifugation at 39 000 g, 4 ºC for 30 minutes.

For protein precipitation ammonium sulfate is used, with concentration up to 0.23 g/ml to remove fraction without FNR1, and up to 0.4 g/ml for salting out FNR1 to pellet. This step was controlled by use of SDS-PAGE. Ammonium sulfate is added under stirring under a 30 min time interval for each desired concentration. Pellets are formed by centrifugation at 39 000 g, 4 ºC for 20 minutes.

Before desalting by size exclusion chromatography, the protein precipitate is dissolved in 3ml buffer A (See appendix). Dissolving was done while being kept on ice and after filtrated by 0.45 syringe-filter. For desalting a 5 ml HiTrap desalting column (see appendix) was used on the AKTA purifier system equilibrated in buffer A. Protein absorption at 280nm and 450nm was used to select desired fractions.

Ion exchange chromatography was performed with anion-exchange column (HiTrap Q HP, Cyvita) and AKTA purifier system using buffer A and Buffer B (See appendix). After performing a test run to find possible optimization steps the purifications were done with a concentration gradient of buffer B going from 18% to 40%. Fractions are selected by use of absorption at 280nm and 450nm.

Gel filtration chromatography was done with size exclusion column Superdex 200 (GE Healthcare) and HEPES buffer (See appendix). Fraction selection by use of absorption at 280nm and 450nm. After filtration the protein is concentrated by use of Amicon Ultra 10k/30k centrifugal filters and centrifugation at 5000 x g for 10 minutes at 4 ºC.

2.4. Sodium dodecyl sulphate- & native- polyacrylamide gel electrophoresis

Principle

Both Sodium dodecyl sulphate- & native- polyacrylamide gel electrophoresis (SDS-PAGE and Native-PAGE) are methods used to find size of protein fragments and utilize the same principle of using an electric field and a polyacrylamide gel. The protein fragments are charged and the electric field act as a driving force, making the proteins move towards the anode. The gel provides resistance when moving and larger proteins will provide greater resistance and therefore move more slowly through the gel. To identify proteins by size a standardized sample is loaded together with the protein sample. This makes it possible to compare sample protein with known values [24].

Sodium dodecyl sulphate (SDS) used in SDS-PAGE is an anionic detergent and is used to coat the protein to produce an even charge across the length of the proteins. During SDS-PAGE the protein is only separated by charge. For Native-PAGE the protein migration rate is dependent on both charge and structure. During Native-PAGE the samples are prepared in a non-denaturated and non-reducing buffer as opposed to SDS-PAGE.

Procedure

For SDS-PAGE protein samples were loaded with NuPAGE LDS Sample Buffer (4x) (Invitrogen) in a 3:1 ratio and set on a heat block at 96 ºC for 5 minutes. The samples were loaded together with a protein marker (SeeBlue Plus2 Pre-Stained Protein Standard (Invitrogen)) on a NuPAGE Bolt 4-12% Bis-Tris, 1.0 mm, Mini Protein Gel (Invitrogen). The electrophoresis was done at 200 V for 20 minutes (Pharmacia Biotech EPS 600) and gel was stained in InstantBlue buffer (See appendix).
For Native-PAGE the protein samples were loaded with NativePAGE Sample Buffer (4x) (Invitrogen) in a 3:1 ratio. The front and back chamber was filled with Anode buffer (See appendix) and middle chamber filled with light blue cathode buffer (See appendix). Electrophoresis was done at 150 V for 115 minutes (Pharmacia Biotech EPS 600). Gel was treated with Fix solution (See appendix) for 15 minutes before left in Destain solution (See appendix) for 24 hours.

2.5. Crystallization and buffer screen

Principle

Protein crystallization is the process of making protein molecules stabilized in a crystal formation. If the crystal is sufficiently ordered diffraction is possible, which allows X-ray crystallography to determine the structure of the protein [25].
For crystallization to occur the protein needs to go through a nucleation phase and a growth phase. For this to happen the protein concentration and precipitating agent concentration must be selected such that the solution starts in the nucleation/labile phase and then transfers to the growth/metastable phase (figure 4). Supersaturation is used to cause crystallization and a balance must be found between too high protein concentration where precipitation occurs, and a too low concentration where the solution is stable. Vapor diffusion is a common method of crystallization, where both sitting drop method and hanging drop method utilize the principles of vapor diffusion. Sitting drop method, which is the method used in this project, is done by putting a crystallization droplet with protein and some precipitation agent on a bridge above the reservoir buffer solution (Figure 5). Water equilibrium between the mixed drop and the reservoir will increase concentration of protein and precipitation agent in the drop, hopefully causing the solution to enter the nucleation phase and start forming crystals. As crystals are formed the protein concentration is reduced and the solution enters the growth phase.

Besides protein concentration and precipitation concentration, other factors also affect crystallization. These are factors such as ionic strength, pH, temperature, additives, impurities, etc. In order to find a solution that gives crystallization a crystallization screening is performed, where a series of different conditions are tried to see where crystals are formed. After a wide screening the buffer can be further optimized from conditions where crystals were formed.

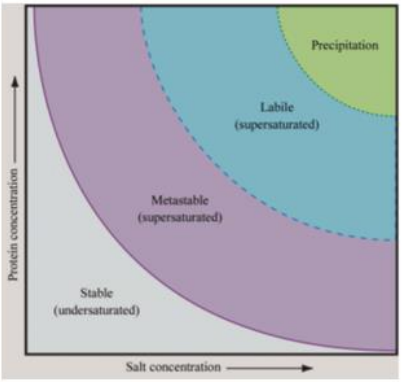

Figure 4 - Phase diagram for crystallization of proteins. The diagram shows the different phases based on concentration of protein and salt with an equilibrium between the phases. Figure from [24].

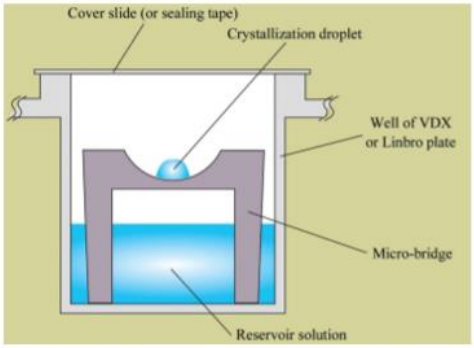

Figure 5 - Sitting drop crystallization where a droplet of protein mixed with solution is put on a bridge above reservoir solution. Water equilibrium will cause concentration to increase which allows the protein to crystallize. Figure from [24].

Procedure

All initial crystallization screen were performed using a Mosquito crystallization robot (SPT Labtech) with crystallization screens Morpheus (Molecular Dimensions) and SaltRx (Hampton Research). For initial screening 1.1 mM protein with 250 nl droplets were used. After crystallization occurred in SaltRx and Morpheus optimizations were done for the conditions giving successful results (G8 for Morpheus and F12 for SaltRx) [26] [27]. For both optimizations the selected method was sitting drop method done at room temperature. 1 µl 1.1 mM of protein was mixed with 1 µl of crystallization solution on a bridge above 100 µl reservoir of crystallization solution. For Morpheus, eight drops with protein concentration at original level and halved concentration with four different precipitant concentrations ranging from 100% to 70% of original concentration. For SaltRx, 64 drops with changes to precipitation agent and concentrations ranging from 100% to 70%. Protein concentration was kept constant while salt concentration was tested in a range of 1.4 M to 1.6 M and pH tested in the range of 7.5 to 8.5.

2.6. X-ray crystallography

Principle

X-ray crystallography is a method of determining structure of a crystal by use of diffraction. The crystal is irradiated by X-rays which diffracts into different directions. This is done while rotating the crystal, obtaining the diffraction from different angles. When the crystal is radiated by X-rays the electrons oscillate and radiate in all

directions. The rays from each electron in the crystal structure interact, and electromagnetic waves can be recorded by a detector. The waves hitting the detector can be described by the following parameters: frequency, amplitude, and phase. By combining the information from the waves at each angle a diffraction pattern can be made. Measuring the diffraction pattern and intensities of radiation makes it possible to decipher the structure of the crystal.

Procedure

Crystals were gathered from the conditions of both Morpheus and SaltRx. Before transferring the crystal to site for X-ray crystallography the crystals were selected, frozen and kept on storage with liquid nitrogen. For crystals made with SaltRx conditions, 25% glycerol was added to prevent the formation of ice crystals. Morpheus screen comes with cryo solution preventing formation of ice crystals and no glycerol was added here. Crystals were collected and sent for diffraction. Diffraction was done at ID30B at the European Synchrotron Radiation Facility (ESRF), Grenoble. Diffraction images were auto-processed by autoPROC [28] and XDS by MxCube software system [29] at the ESRF, before further processing and refinement by use of the CCP4 package and COOT [30] [31].

The program AIMLESS was used to process unmerged intensities and find symmetries, scale the data and making sure reflections collected several times are combined [32]. PHASER [33] was used to solve the structure with molecular replacement. REFMAC [34] was used for restrained refinement including jelly-body and non-crystallographic symmetry restraints, and COOT used to view coordinates and manually adjust the structure. During the refinement cycles R factor and Rfree values were monitored and refinement controlled by Ramachandran plot and multimeric model geometry validation. During deciphering of crystal structure 2 slightly different rotations was found and required different methods to be solved. The first structure was solved by use of PDBid 6GAR as a dimer [6]. For the other structure PDBiD 6GAR was first split into its NADPH- and FAD domains of the monomer, and the structure was solved by searching initially for 8 of these domains.

2.7. Kinetic studies – Electron transfer

Principle

To compare characteristics of $FNR1_{mutant}$ in regard to electron transfer an assay can be performed. FNR1 is able to reduce Flds and FDs by use of NADPH as an electron donor and by comparing the rate this is happening at when looking at $FNR1_{wild\ type}$ vs $FNR1_{mutant}$ will indicate efficiency and turnover. The FAD cofactor in FNR1 is continually working as a reduction agent for NrdI/Fld2 and is itself reduced by NADPH. During the experiment NrdI/Fld2 will be reduced and FMN will change oxidation state, going from oxidized to semiquinone and hydroquinone form. The difference in light absorption between the different oxidation states can be used to determine concentrations. For this to be possible FMN cannot be allowed to go back to oxidized form by reacting with oxygen. The experiment must therefore be performed in anaerobic conditions and a glovebox with an inert gas can be used.

Procedure

All kinetic measurements were done in a glovebox without oxygen present (91% N_2, 9% H_2, AGA) (Plas-Labs Anaerobic Chamber 855-AC with Agilent 8453 diode-array UV-vis spectrophotometer). NrdI, Fld2 and $FNR1_{Wild\ type}$ was available from earlier experiments. A Tris-HCl buffer (See appendix) was used, with 200 µM NADPH, 5 µM FNR1, and varying the concentration of NrdI and Fld2 between 0.5 µM and 30 µM. The components were added to a quartz cuvette with stirring and light absorption recorded every 0.5 s for 20 minutes, for selected wavelengths to determine concentrations. Oxidized form of FMN with λ_{max} peaks at 447 nm ($NrdI_{ox}$) and 459 nm ($Fld2_{ox}$) while semiquinone form with λ_{max} peaks at 575 nm ($NrdI_{sq}$), 592 nm ($Fld2_{sq}$), and 800 nm was used as a baseline value. For NrdI and Fld2 ε has been determined to be 10.8 $mM^{-1}cm^{-1}$ with concentration determined by Beer-Lambert Law [6]. To determine the steady state kinetic parameters the concentrations were plotted as a function of time. The initial slope could be estimated from the plots of the $NrdI_{ox}$ and $Fld2_{ox}$ reduction as function of time for the different substrate concentrations used. Initial reduction rates were plotted against concentration by using the Michaelis-Menten function using Origin (Origin Lab Corporation) giving values for V_{max}, k_{cat} and Km.

3 Results and discussion

3.1. Bacterial transformation

The plasmid containing the gene for FNR1 with val329 mutated to his329 was successfully transformed into competent BL21 cells (Novagen). After transformation bacterial culture was grown in tubes of LB-medium before samples were plated on agar plates with ampicillin. For each agar plate 2 bacterial colonies selected from the plates and after overexpression of protein by bacterial growth SDS-PAGE tests were done (Figure 6 & Table 2). Each bacterial colony shows successful transformation of *B. cereus* as evident by the expression of FNR1. A standardized sample with proteins of known mass was used to determine size. FNR1 has a molecular mass of 36 kDa and the presence of a band in this range indicates successful transformation for all bacterial colonies.

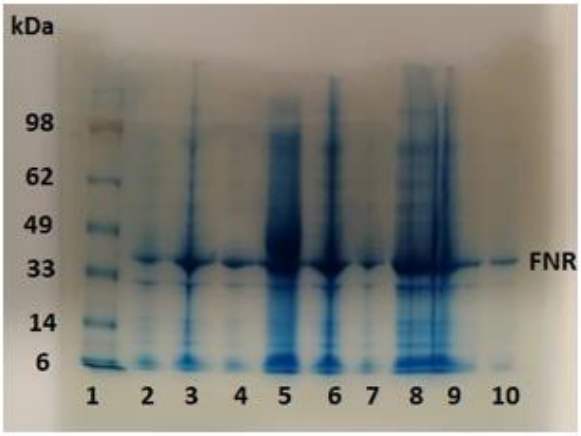

Figure 6 - SDS-PAGE of protein expression after transformation of cells. Standardized sample, sample before induction and samples for bacterial colonies (table 1). FNR1 expected at 36 kDa.

Table 2 - SDS-PAGE of protein expression after transformation of cells. Transformed bacteria were plated on agar plates from 4 tubes of LB-medium and 2 colonies selected from each plate.

1	Standardized sample
2	Before IPTG
3	Tube 1
4	Tube 1, colony 2
5	Tube 2
6	Tube 2, colony 2
7	Tube 3
8	Tube 3, colony 2
9	Tube 4
10	Tube 4, colony 2

3.2. Protein purification

After transformation large scale bacterial growth was conducted for overexpression of protein. Large scale bacterial growth was done in 2 operations, but the first batch of bacterial growth gave a low yield and optimization was done before 2nd batch of bacterial growth. For 2nd batch growth temperature was reduced from 37 ºC to 30 ºC for pre-induction step, cultures were cooled briefly on ice prior to induction with IPTG, and further grown at 18 ºC over night.

First step of protein purification was done by ion exchange chromatography (IEX). IEX chromatograms (figure 8-10) shows a clear peak for 450 nm which made separation of FNR1 possible. The peak at 450 nm overlaps with wavelength 280 indicating other proteins in solution and some impurities will stay in separated solution. First purification run (Figure 8) was conducted where Buffer B (see appendix) concentration was slowly increased from 0% to 40%. For following runs optimizations were done and salt concentration going from 18% to 40%.

For optimized runs (Figure 9 & Figure 10), the salt gradient was adjusted, making separation of FNR1 better by making the 450 nm peak more distinct. After IEX increased purity can be seen in SDS-PAGE (Figure 7 and table 3) as the band at 36 kDa becomes more distinct while the other bands fade out, indicating a higher relative concentration of FNR1.

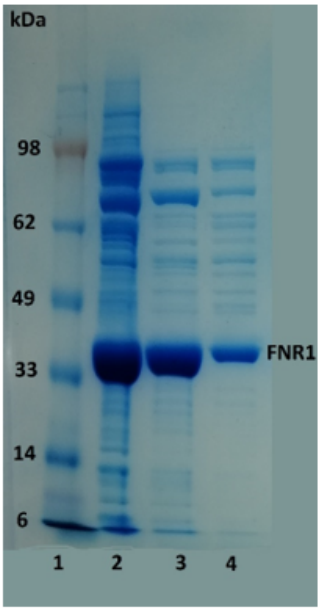

Figure 7 – SDS-PAGE of protein purification. Standardized sample, sample before purification and after performing IEX and SEC (table 3). FNR1 expected at 36 kDa

Table 3 - SDS-PAGE of protein purification

1	Standardized sample
2	Before purification
3	IEX
4	SEC

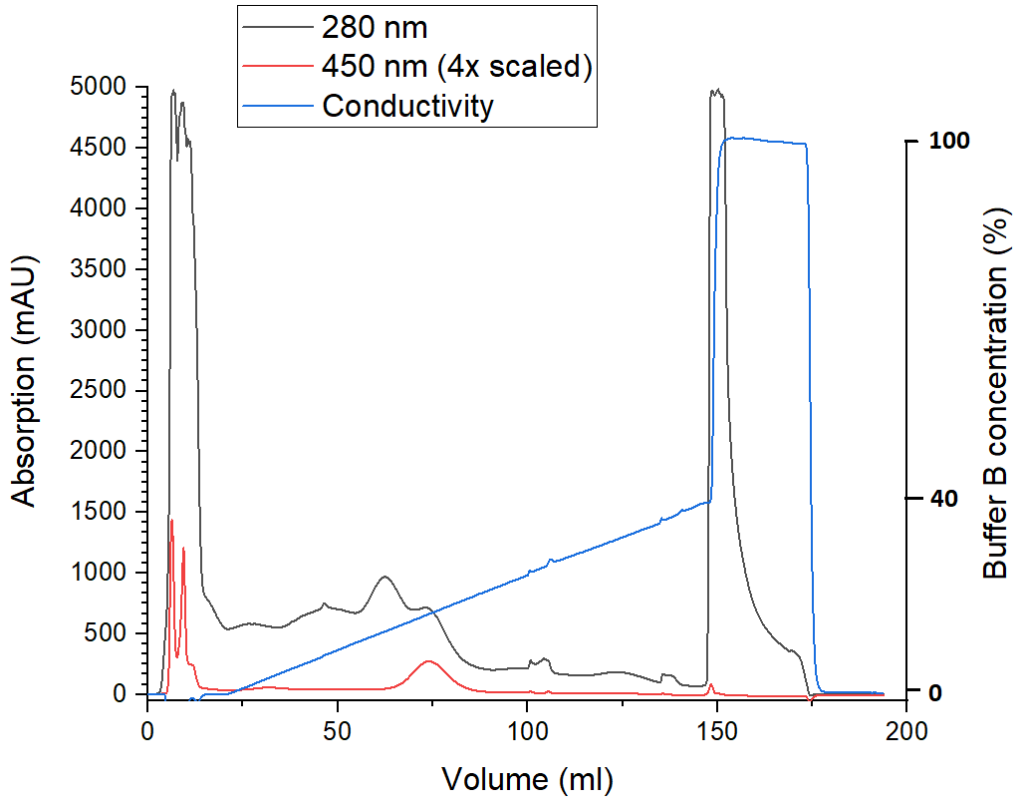

Figure 4 - IEX chromatogram for 1st bacterial batch. Absorption line for 450 nm is scaled 4x. Absorbance for 450 nm and 280 nm was recorded as a function of volume and fractions separated based on FNR1s absorption at 450 nm.

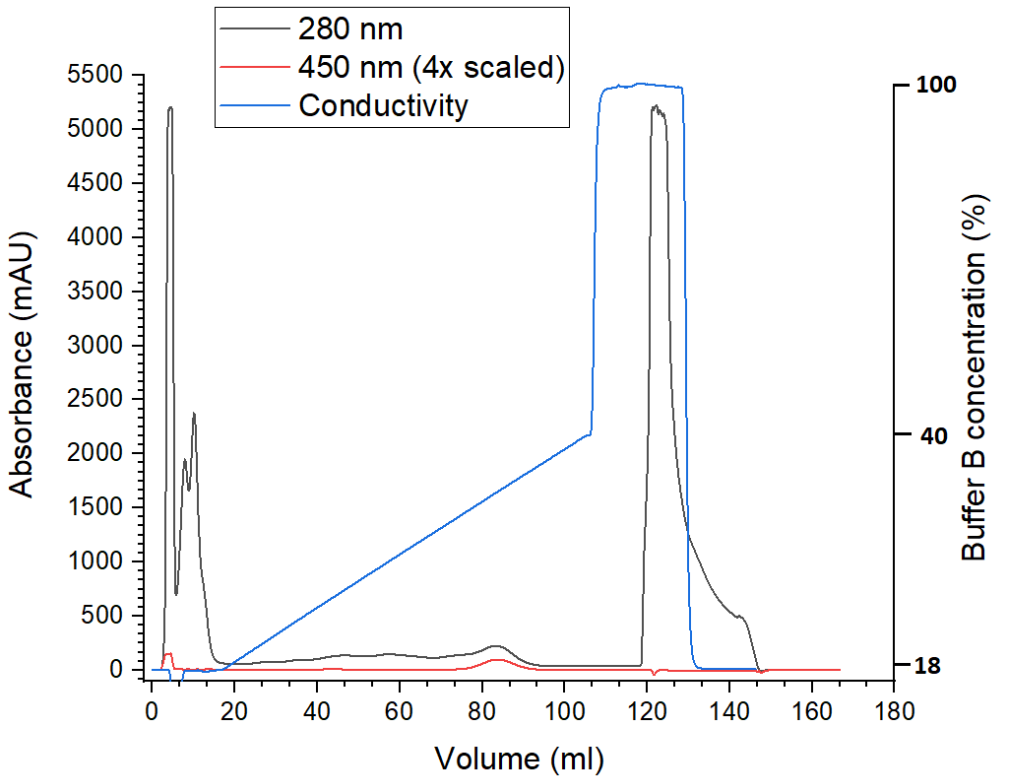

Figure 9 - IEX chromatogram for 1st bacterial batch after optimizing. Absorption line for 450 nm is scaled 4x. Absorbance for 450 nm and 280 nm was recorded as a function of volume and fractions separated based on FNR1s absorption at 450 nm.

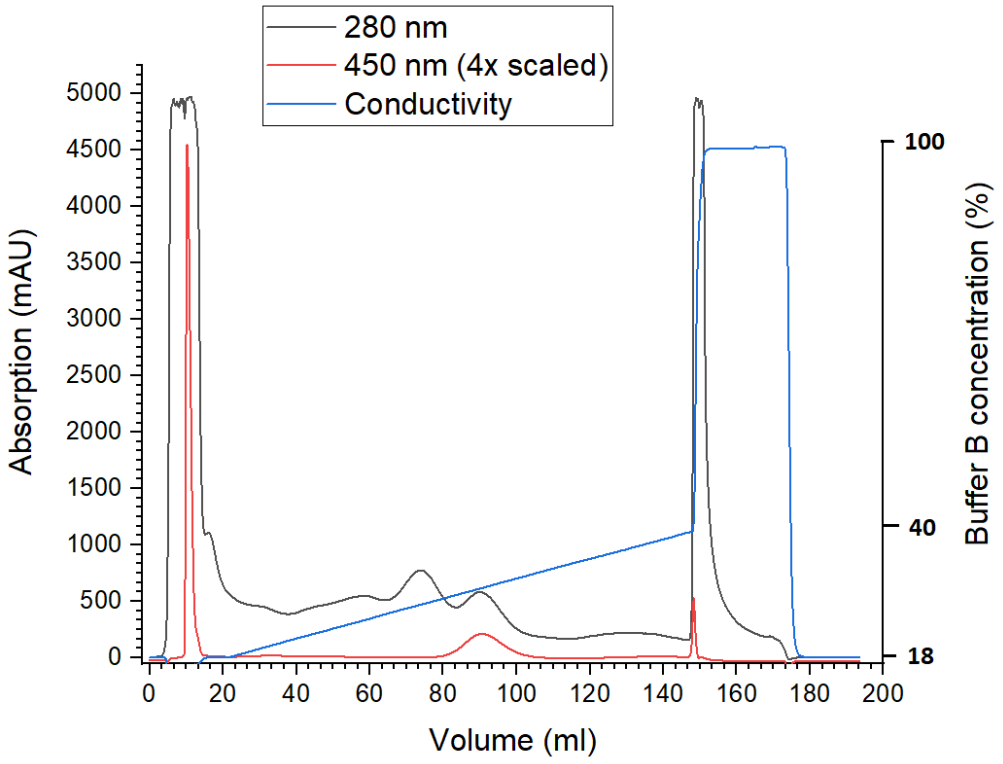

Figure 10 - IEX chromatogram for 2nd bacterial batch after optimizing. Absorption line for 450 nm is scaled 4x. Absorbance for 450 nm and 280 nm was recorded as a function of volume and fractions separated based on FNR1s absorption at 450 nm.

After IEX the protein samples underwent SEC, where separation was done based on size and time for elution (figure 11 & figure 12). Samples were selected based on absorbance at 450 nm due to FNR1 absorbing light in this wavelength. The purification was done separately for 1st and 2nd bacterial batch, and the first batch shows some error in having a peak at 280 nm before the 450 nm peak. This peak indicates some protein with high absorption in the 280 range but with no absorption in the 450 nm range. This could be apoprotein, but the source of this peak was not examined. The 2nd bacterial batch shows a clearer peak, and for the growth of this batch some changes was done which might explain the differences in absorption. For the 2nd batch a lower temperature was used, and an ice bath before inducing with IPTG.

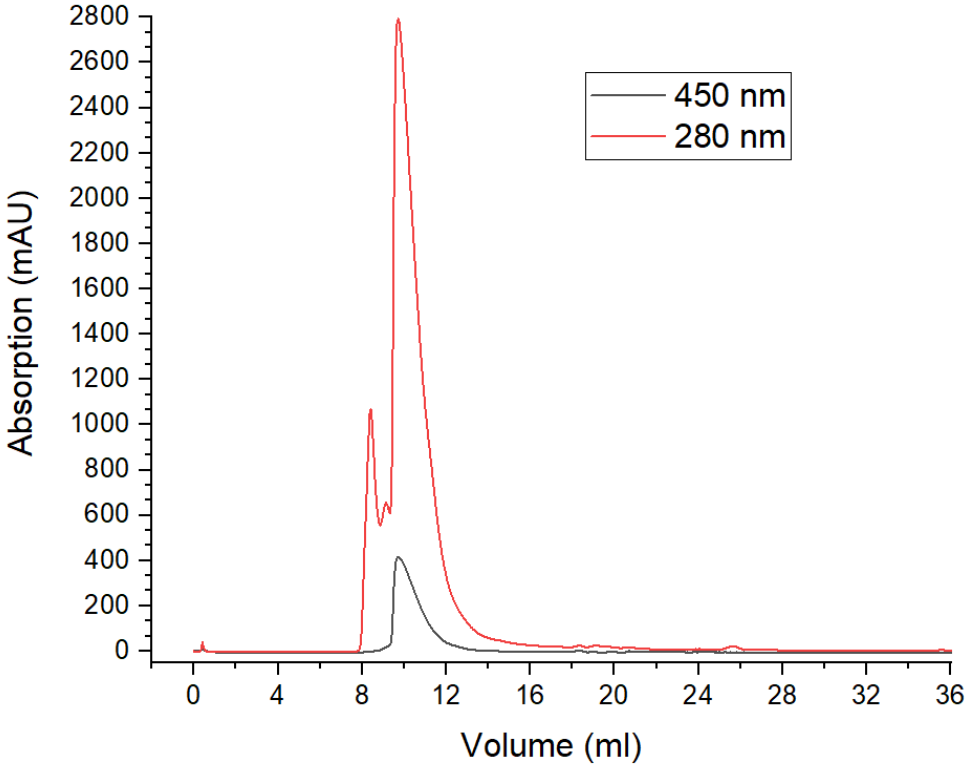

Figure 11 - SEC chromatography for 1st bacterial batch. Absorbance at 450 nm and 280 nm was recorded as a function of volume and fractions separated.

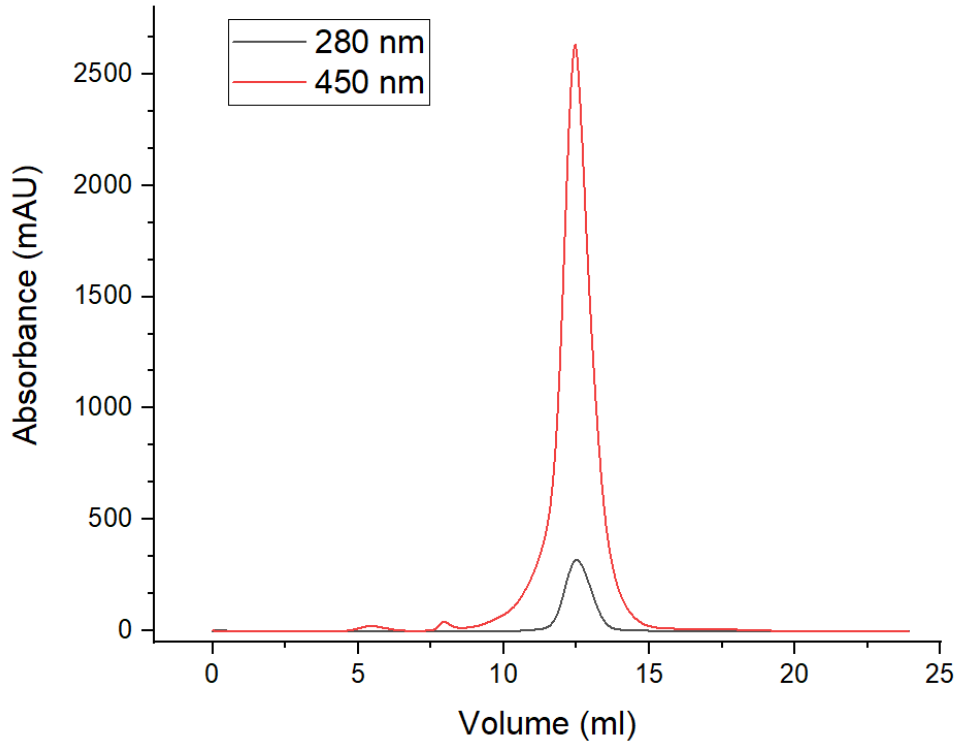

Figure 12 - SEC chromatography for 2nd bacterial batch. Absorbance at 450 nm and 280 nm was recorded as a function of volume and fractions separated.

3.3. Native-PAGE

Native-PAGE was performed on $FNR1_{mutant}$ in order to investigate the oligomerization state. The protein weight of $FNR1_{mutant}$ is 38.6 kDa for each chain, and 77.2 kDa in dimer structure. A band can be observed in the ~ 77 kDa range which indicates the presence FNR1 as a dimer, which is the same for $FNR1_{wild\ type}$ (figure 13).

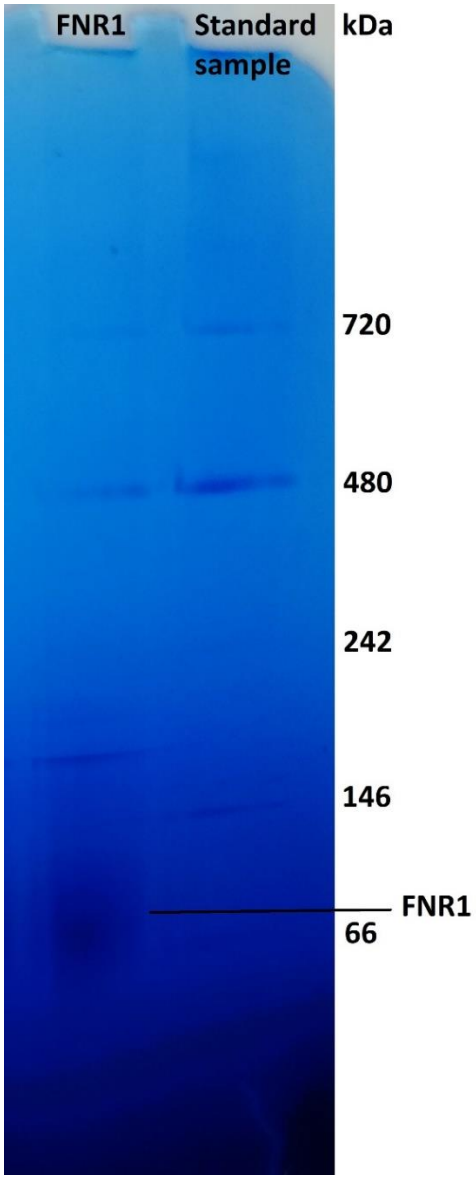

Figure 13 - Native-PAGE with standard sample (Invitrogen) and FNR1.

3.4. Crystallization and structure

During crystallization in commercial screens Morpheus and SaltRx crystallization occurred at 0.1 M carboxylic acid and 0.1 M buffer system 2 and 37.5% v/v precipitant mix 4 at pH 7.5 for Morpheus. For SaltRX crystallization occurred at 1.5 M lithium sulfate in 0.1 M Tris-HCl buffer at pH 8.5 for SaltRx [27] [26]. Further optimization was done where concentrations for protein and solution was changed for Morpheus and concentrations of buffer and pH changed for SaltRx (See methods). On both optimizations more crystals were found and a total of 10 crystals from both optimizations were sent to diffraction.

During crystallization of FNR1, 2 different forms of crystals were observed, furthermore referred to as “diamond shape” and “cube shape” based on their crystal form seen in the microscope. The diamond shape occurred in conditions from SaltRx, while the cube shape originated in the Morpheus conditions. The cube shaped crystal has diffracted to a better resolution and the mutation can more clearly be seen (figure 14 and figure 15). The diamond shaped crystal has lower resolution and the mutation is harder to confirm (table 4), but it has a different conformation and is therefore of interest (figure 17-19). The diamond shape conformation differs with the NADPH domain being slightly rotated relative to the FAD domain. Table 4 shows values for crystal data collection and refinement statistics.

Table 2 - Crystal data collection and refinement statistics for $FNR1_{mutant}$ cube shape and $FNR1_{mutant}$ diamond shape

	Cube shape	Diamond shape
Data collection		
X-ray source	ID30, ESRF	ID30, ESRF
Wavelength (Å)	0.976254	0.976254
Space group	P 21 2 21	I 1 2 1
a, b, c (Å)	56.9, 94.4, 164.6	191.9, 212.5, 192.2
α, β, γ (deg)	90, 90, 90	90, 90, 90
Rotation range per image (deg)	0.05	0.05
Total rotation range (deg)	97	93
Mosaicity (deg)	0.06	0.21
Resolution range (Å)	53.87 - 2.90	47.9 - 3.85
Total no. of reflections	106 735	171 404
Unique reflections	19591	51423
R_{meas}	0.090 (0.303)	0.211 (1.514)
R_{merge}	0.073 (0.252)	0.159 (1.090)
Completeness (%)	96.6 (98.0)	98.9 (99.9)
Multiplicity	5.4 (5.7)	3.3 (3.5)
I/σ (I)	22.1 (5.2)	10.5 (1.0)
$CC_{1/2}$	0.995 (0.963)	0.992 (0.570)
Refinement Statistics		
R_{work}/R_{free}	0.190 / 0.247	0.257 / 0.324
Mean overall isotropic B factor (Å²)	195.59	71.43
Protein assembly in asymmetric unit (AU)	1 dimer	4 dimers
Protein residues by chain	349	349
protein residues	698	2792
Modell ligands	2FAD	8FAD
Added waters	10	247
Ramachandran plot: most favored/allowed/outliers (%)	89.39/9.74/0.87	73.26/19.26/6.98
RMSD bond lengths (Å)	0.0138	0.0153
RMSD bond angles (deg)	1.93	2.08
Estimated overall coordinate error based on maximum likelihood (Å)	0.28	0.87

Cube shape

For the cube shape the assymetric unit is a dimer with a FAD-domain and a NADPH-domain. The space group of the cube shape was identified as P 21 2 21. $FNR1_{mutant}$ from cube shape modelled with electron density map (figure 15) shows the presence of his329. Comparing the structure of $FNR1_{mutant}$ and $FNR1_{wild\ type}$ from 6GAR PDBid shows near identical structure (figure 16).

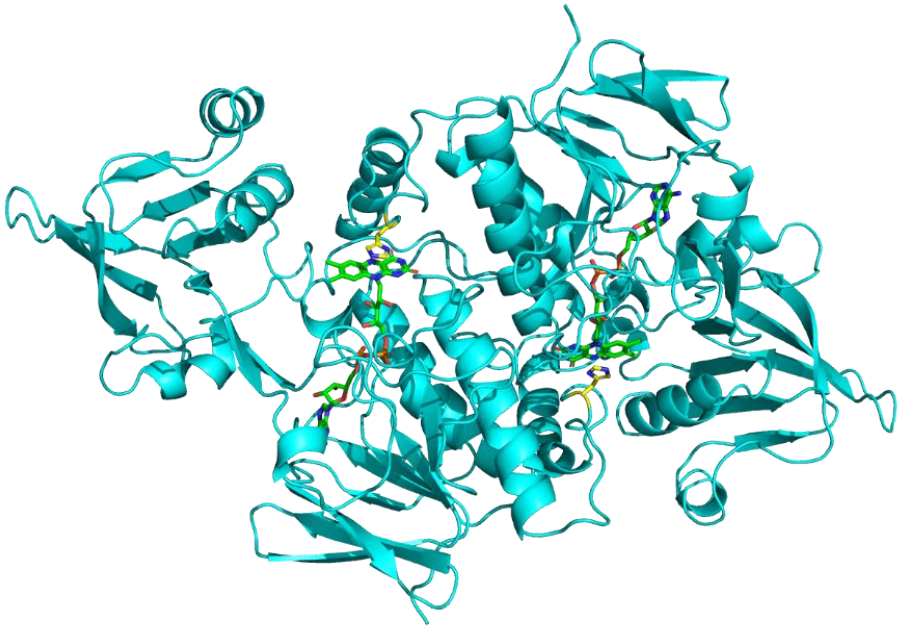

Figure 14 - Structure of FNR1$_{mutant}$ with cofactor (green) and mutation (yellow). From cube shape

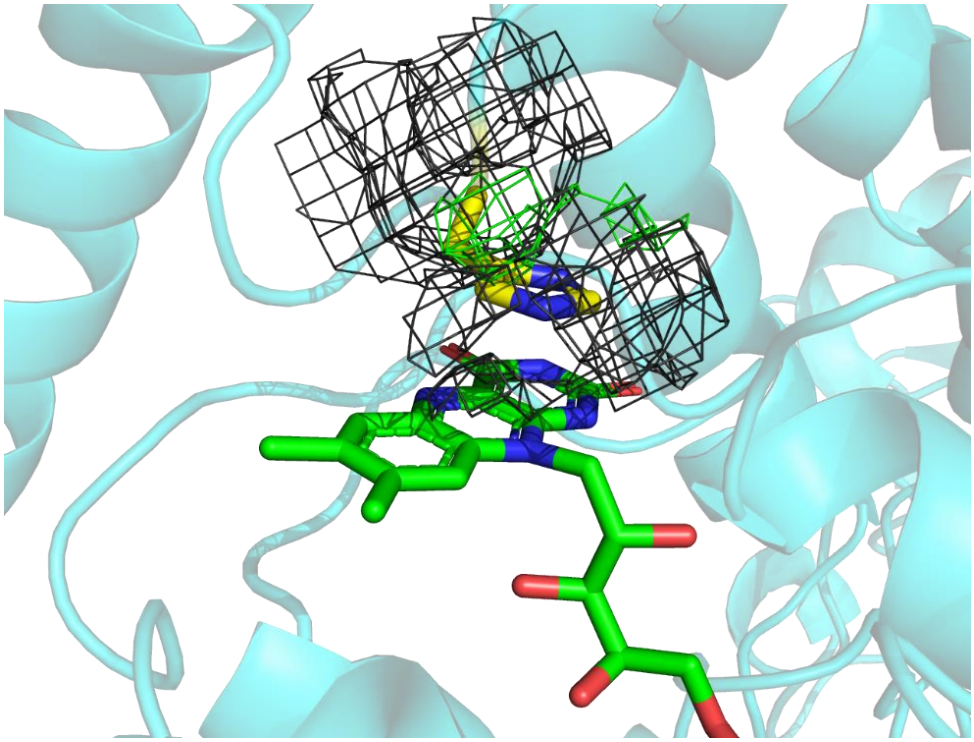

Figure 15 - Structure of FNR1$_{mutant}$ with cofactor (green) and mutation (yellow). Close up image of mutation spot. The electron density maps 2fofc contoured at 1σ, fofc contoured at +3σ and -3σ.

Cube shape and wild type FNR1

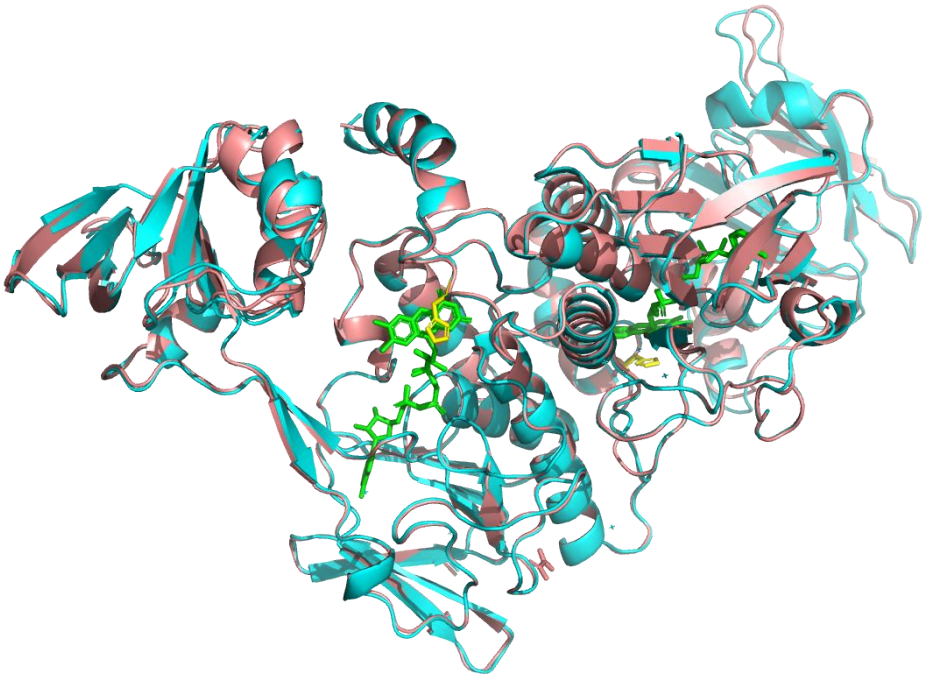

Figure 16 – Structure of cube shape FNR1$_{mutant}$ (light blue) and previously solved FNR1$_{wild\ type}$ (light red). FNR$_{wild\ type}$ from PDBid 6GAR

For FNR1$_{mutant}$ from cube shape the overall structure remains unchanged appart from mutation of val329 to his329 (figure 16).

Diamond shape

For the diamond shape the assymetric unit is 4 dimers with a FAD-domain and a NADPH-domain while the biological assembly consists of one dimer (figure 17). The space group for diamond shape was identified as I 1 2 1. FNR1$_{mutant}$ is modelled with electron density map (figure 18), and while his329 is modelled inn, the resolution is a bit low. The main point of interest for the diamond shape FNR1$_{mutant}$ is the conformation difference from the cube shape and FNR1$_{wild\ type}$ (figure 20). For diamond shape the NADPH-domain is rotated relative to the FAD-domain. FNR1$_{mutant}$ has a different conformation than FNR1$_{wild\ type}$, but the conformation is not closer to the structure of FNR2 which naturally has histidine in position 329 (figure 21).

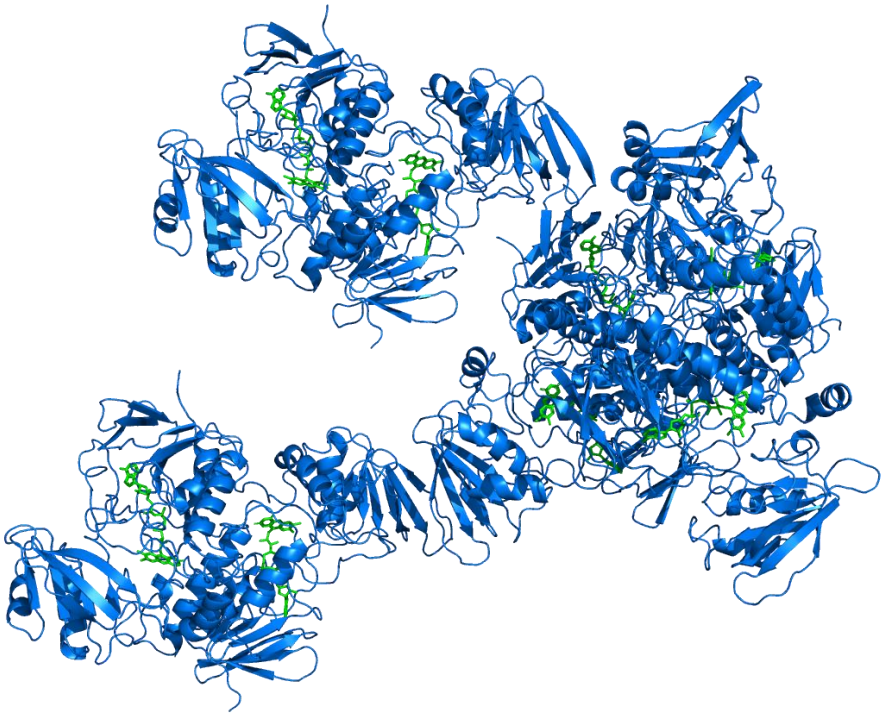

Figure 17 – Structure of FNR1$_{mutant}$ from diamond shape with cofactor (green). Asymmetric unit with 4 dimers. All 8 chains are shown.

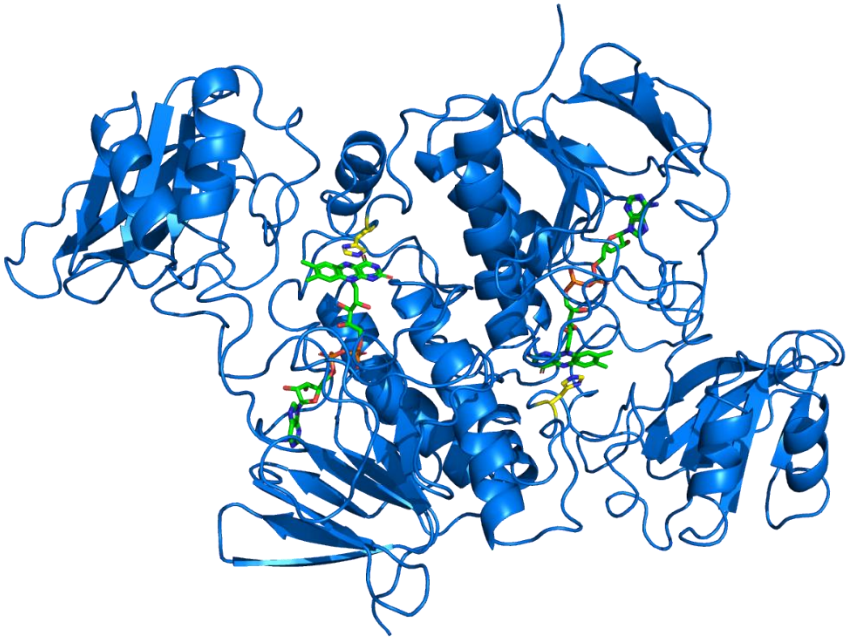

Figure 18 - Structure of FNR1$_{mutation}$ with cofactor (green) from diamond shape. 2 chains shown.

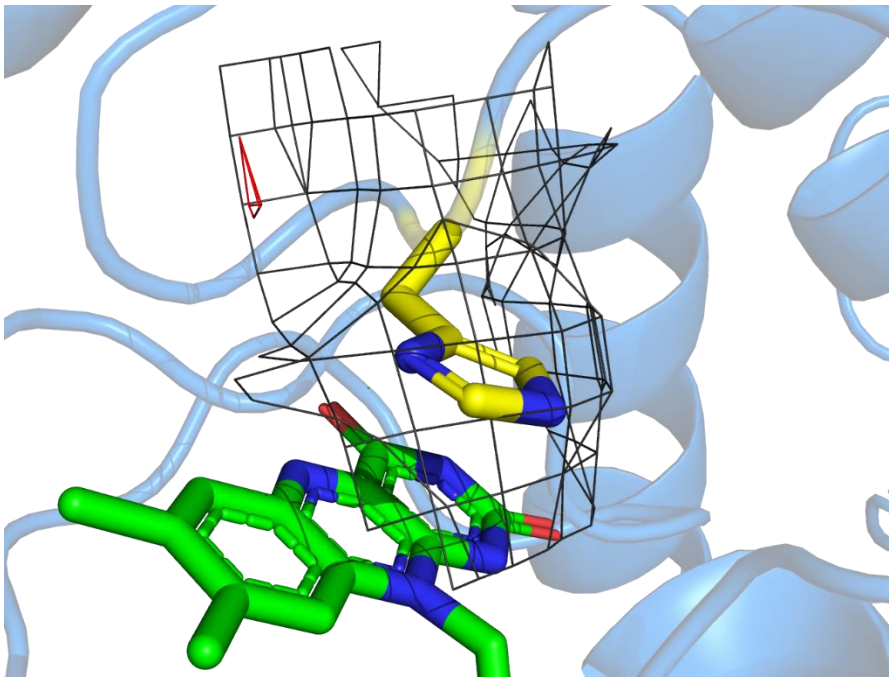

Figure 19 - Structure of FNR1$_{mutation}$ diamond shape. Cofactor (green) and mutation (yellow) marked. 2 chains shown. Close up image of mutation spot. The electron density maps 2fofc contoured at 1σ, fofc contoured at +3σ and -3σ.

Diamond shape and cube shape – overlay

When overlaying FNR1$_{mutant}$ cube shape with FNR1$_{mutant}$ diamond shape a difference in conformation is shown. Diamond shape has a rotation in the NADPH-domain relative to the cube shape and wild type shape (figure 20). Comparing Cube shape and diamond shape to FNR2, the diamond shape rotation does not seem to have made the structure more similar to FNR2 (figure 21).

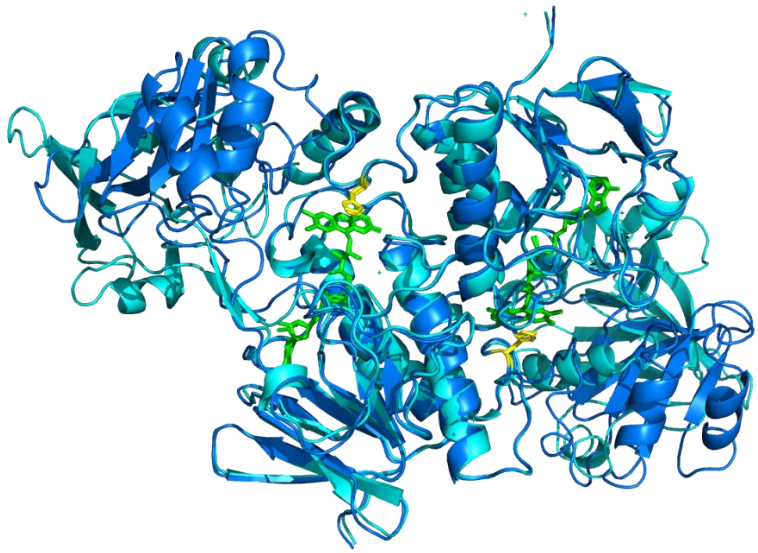

Figure 20 - Structure of FNR1 with cofactors and mutations. Cube shaped (light blue) and diamond shaped (dark blue) with cofactor (green) and mutation (yellow).

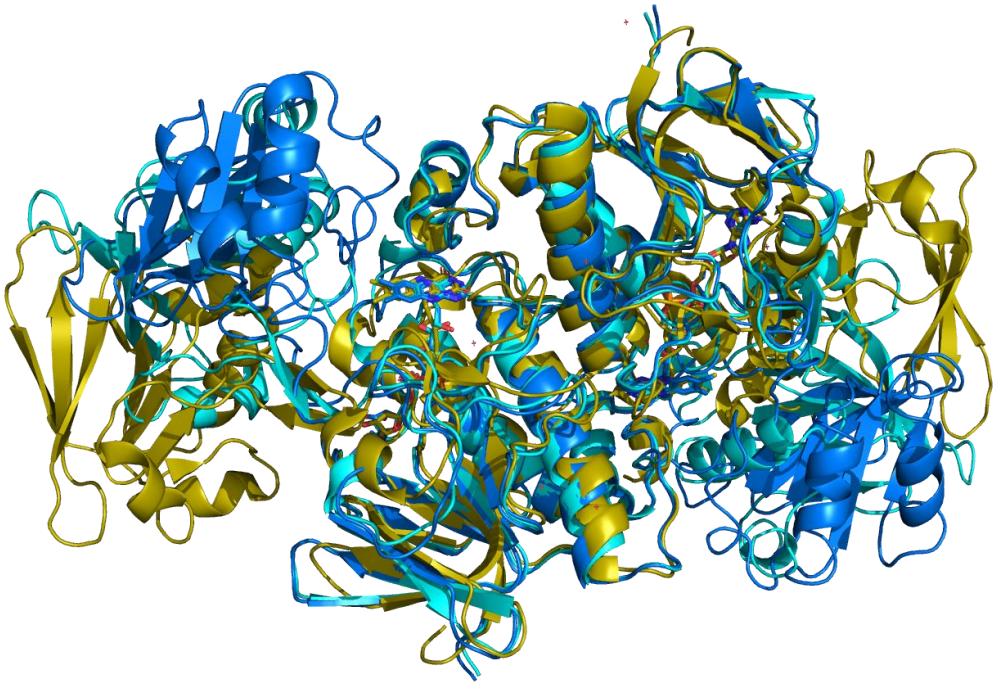

Figure 21 - Structure of FNR1 cube shape (light blue), FNR1 diamond shape (dark blue) and FNR2 (yellow).

Data for crystal collection and refinement (table 4) are satisfactory but not optimal. The resolution range for especially diamond shape is on the lower side, and the Ramachandran plot for both structures have a few outliers. The structures do have decent values for overall coordinate error based on maximum likelihood, good values for completeness and good values for R_{meas} and R_{merge}.

3.5. Electron transfer

To survey FNR1s ability to reduce Fld2 and NrdI kinetic studies were performed with both $FNR1_{mutant}$ and $FNR1_{wild\ type}$. With NrdI as substrate (figure 22), activity measurements were only done with $FNR1_{mutant}$, while data for $FNR1_{wild\ type}$ was taken from earlier experiments [6]. Only $FNR1_{mutant}$ was freshly prepared for these experiments, while NrdI, Fld and wild type FNR1 has been stored at -80 ºC for 3-5 years.

NrdI as a substrate

$FNR1_{mutant}$ was able to reduce NrdI but was shown to perform worse than $FNR1_{wild\ type}$. For NrdI the $FNR1_{mutant}$ shows a k_{cat} value 4-fold lower than the wild type (Table 5) while the K_m value is slightly higher for the mutant. The big difference in k_{cat} indicates that the mutation made FNR1 a worse redox partner for NrdI. Meanwhile the increase in K_m for the mutation can indicate that mutating val329 to his329 makes FNR1 have a slightly lower affinity for NrdI. This is a weak increase and within range of error, and no hard conclusions can be drawn. Looking at k_{cat} / K_m, $FNR1_{mutant}$ is shown to be slightly less efficient than wild type FNR1 with $FNR1_{mutant}$ having 6-fold lower k_{cat} / K_m. Comparing the values for $FNR1_{mutant}$ the values are far from $FNR2_{wild\ type}$ where histidine is found naturally. $FNR1_{mutant}$ has a lower k_{cat} value, and did not significantly increase K_m.

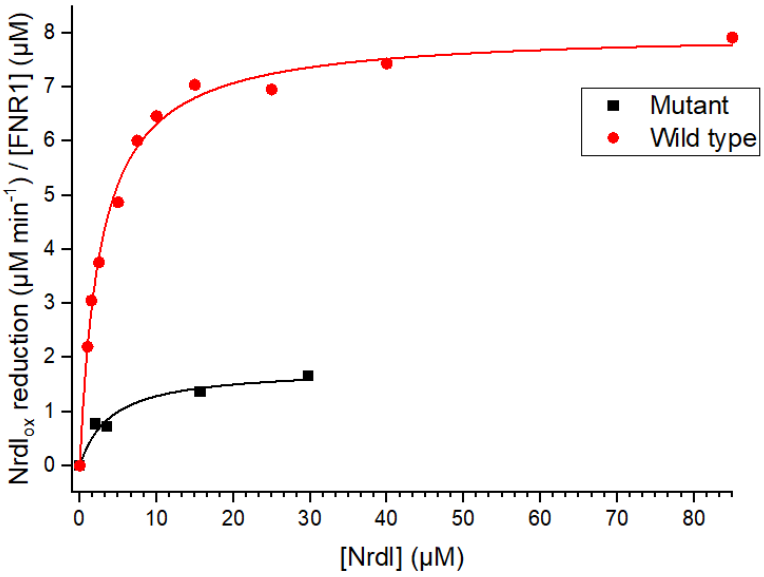

Figure 22 - Steady-state reduction of NrdI by FNR1. Variable concentrations of NrdI, 200µM NADPH, and 0.5 µM FNR1. Data fitted with the Michaelis-Menten function.

Table 5 - Steady state kinetic parameters for the reduction of NrdI by FNR1. Results from $FNR1_{Wild\ type}$ and $FNR2_{Wild\ type}$ taken from Gudim Et Al. [6]

	k_{cat} (min^{-1})	K_M (µM)	k_{cat} / K_m (µM^{-1} min^{-1})
$FNR1_{mutant}$	1.8 ± 0.2	4.0 ± 1.3	0.5 ± 0.2
$FNR1_{Wild\ type}$	8.0 ± 0.1	2.7 ± 0.2	3.0 ± 0.4
$FNR2_{Wild\ type}$	100 ± 4	61 ± 5	1.6 ± 0.2

Fld2 as a substrate

For Fld2 (See appendix) kinetic studies were done for both the mutant and wild type FNR1s (figure 22 & table 6). Values for wild type FNR1 was compared to values from results published in 2018 [6]. The difference in data for $FNR1_{Wild\ type}$ and $FNR1_{Wild\ type\ 2018}$ might be due to deteriorating after storage as the results are not completely replicable but show some indications. The difference between the k_{cat} values for Fld2 reduction by FNR1 measured in this work, as compared to the previous study ([6]) are small with a slight decrease for the mutation. K_m shows a noticeable decrease from $FNR1_{Wild\ type2021}$ and $FNR1_{Wild\ type\ 2018}$ with a 2-fold and 5-fold decrease. The differences are still within the same size range and there is some uncertainty for 2018 data, which makes it hard to draw strong conclusions (table 6). Comparing the $FNR1_{mutant}$ to FNR2, k_{cat} has decreased instead of increasing by doing the mutation, and while the mutation has given K_m values closer to FNR2 the difference in values is small with the values being in the same size range.

The $FNR1_{mutant}$ has approximately half the k_{cat} value for both wild type data, and the mutation seems to have reduced the ability to reduce Fld2. For K_m values the mutant has lower values than the 2021 data, which again is lower than the 2016 data (table 6). While the data difference between 2018 and 2021 is not optimal it still shows an indication that the mutation reduced the K_m value. For low concentrations the $FNR1_{mutant}$ works better than $FNR1_{wild\ type}$ with Fld2 as a substrate. The difference in K_m could indicate that the mutation increases the affinity, but no clear conclusion can be drawn. Looking at k_{cat} / K_m values $FNR1_{mutant}$ has the highest values (table 6) despite having the lower k_{cat} values. This makes $FNR1_{mutant}$ a better partner than wild type FNR1 at low substrate concentrations, but less efficient at maximal rate. It must be mentioned that the data for $FNR1_{mutant}$ relies on few data points, and to be able to conclude with more certainty more data points should be taken.

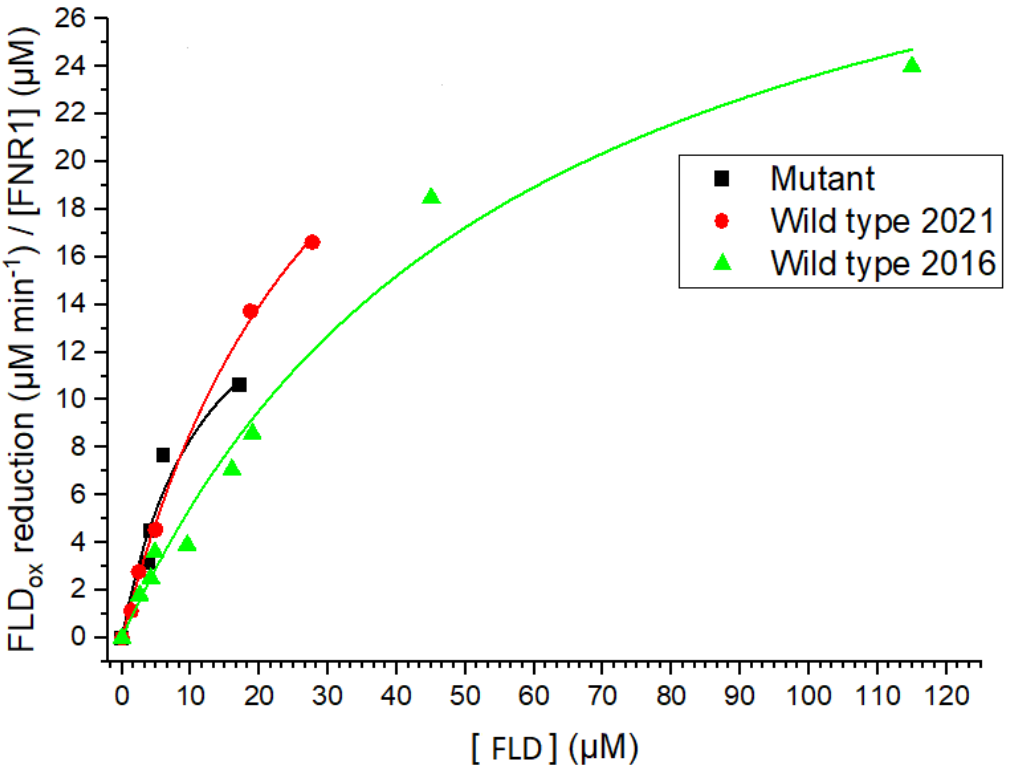

Figure 22 - Steady-state reduction of Fld2 by FNR1. Variable concentrations of Fld, 200µM NADPH, and 0.5 µM FNR1. Data fitted with the Michaelis-Menten function.

Table 6 - Steady state kinetic parameters for the reduction of Fld2 by FNR1. Results from $FNR1_{Wild\ type\ 2016}$ and $FNR2_{Wild\ type}$ taken from Gudim Et Al. [6]

	k_{cat} (min^{-1})	K_M (µM)	k_{cat} / K_m ($µM^{-1}$ min^{-1})
$FNR1_{mutant}$	19 ± 6	12 ± 7	1.5 ± 1.0
$FNR1_{Wild\ type2021}$	36 ± 3	32 ± 5	1.1 ± 0.1
$FNR1_{Wild\ type2018}$	42 ± 8	60 ± 22	0.7 ± 0.3
$FNR2_{Wild\ type\ 2018}$	9125 ± 1450	13 ± 5	701 ± 360

4. Conclusion

4.1. Effect of mutation

The basis of this project was the difference in steady state kinetics between FNR1 and FNR2 and what structural differences might be the source of this. FNR2 using Fld or NrdI has shown to be a much more efficient redox partner [6] and one hypothesis was that this was due to FNR2 having an aromatic residue stacking the FAD cofactor. FNR1 has a valine in position 329, while FNR2 has a histidine, and by mutating FNR1, giving it more of an aromatic character, it is possible to survey the effect of this. If this histidine affects the steady state kinetics of FNR2, $FNR1_{mutant}$ should show changes in values towards what we expect from FNR2.

The mutation of FNR1 was successful and changing val329 to his329 did not seem to affect overexpression of protein or purification, nor protein stability as compared to the wild type FNR1 (previous studies). Crystallization of the $FNR1_{mutant}$ was also successful, with the following processing of data and solving the structures. When it comes to steady state kinetics the mutation shows overall lower k_{cat} values, indicating it has become a worse redox partner. This is counter to what was hypothesized as FNR2 with histidine in position 329 has higher k_{cat} values than $FNR1_{wild\ type}$ [19]. For K_m values it seems like the mutation increased the value for NrdI as a partner but lowered the value with Fld. Looking at k_{cat} / K_m an improvement was shown for Fld as a partner, but a decrease with NrdI.

Comparing $FNR1_{wild\ type}$ with $FNR2_{wild\ type}$ with NrdI as a substrate, FNR2 has higher k_{cat}, higher K_m, but lower k_{cat} / K_m (table 5). By mutating FNR1 one could assume changes towards the values previously observed for FNR2. If his329 is beneficial for the steady state kinetics of FNR2, the mutation should increase k_{cat}, increase K_m, but decrease k_{cat} / K_m (table 5), but this has only partly happened. $FNR1_{mutant}$ has decreased k_{cat}, but increased K_m and decreased k_{cat} / K_m. The mutation seems to not be beneficial for k_{cat} values. When it comes to K_m it could be argued the mutation did as expected and increased the value, but the change here is small and the uncertainty significant, and no strong conclusions can be drawn. Overall $FNR1_{mutant}$

has shown to be overall less efficient than the wild type FNR1 with NrdI as a substrate and the mutation did not seem to have a positive effect.

For Fld2 as a substrate when comparing $FNR1_{mutant}$ with $FNR2_{wild\ type}$, FNR2 has higher k_{cat}, lower K_m, and much higher k_{cat} / K_m (table 6). By mutating FNR1 one could assume changes towards the values of FNR2. If his329 is beneficial for the steady state kinetics of FNR2, the mutation should increase k_{cat}, decrease K_m, but increase k_{cat} / K_m (table 6), but this has only partly happened. $FNR1_{mutant}$ has decreased k_{cat} and k_{cat} / K_m show little difference, but values for K_m has decreased. The mutation seems to not be beneficial for k_{cat} values, but when it comes to K_m it could be argued the mutation did as expected. The values for K_m in $FNR1_{mutant}$ and $FNR2_{wild\ type}$ are within the range of error (table 6) and mutating shows a decrease in K_m from $FNR1_{wild\ type}$. This data relies on too few data points to reach clear conclusions, but this indicates that the mutation might be beneficial for K_m values and substrate affinity. For k_{cat} / K_m the values of $FNR1_{mutant}$ are 480-fold lower than $FNR2_{wild\ type}$, but this is largely due to k_{cat} values. $FNR1_{mutant}$ with Fld2 as a substrate did not give the increased k_{cat} or k_{cat} / K_m that was expected, but the decrease in K_m indicates that histidine plays a role here.

For both NrdI and Fld2 as a substrate, the mutation had opposite effect on k_{cat}, but slight positive effect on K_m, although the certainty is very low for NrdI. FNR1 and FNR2 differs in more areas than just val329 vs his329 and only this mutation is not enough to get more equal kinetic data, but this study could indicate that the histidine plays a role in K_m values and makes the enzyme more efficient at low substrate concentrations. The fact that valine is conserved in FNR1 despite histidine giving lower K_m values can be explained by the mutation giving a decrease in k_{cat}. Val329 might have been under selection for a maximal rate at the expense of K_m and substrate affinity. As the mutation from val329 did improve the K_m values but impaired the k_{cat} value this mutation by itself seems to not be beneficial overall.

Due to how poorly FNR1 works for reducing Flds, both as wild type and after mutation, it could be theorized that FNR1 plays other roles in vitro. Studies on a homologue FNR from *Staphylococcus aureus* shows this FNR playing a crucial role

in iron uptake, where the FNR functions as a reductase for IsdG and IsdI, two heme degrading enzymes [35]. FNR1 from *B. cereus* could play a similar role, and perhaps be more beneficial for reduction of FDs.

4.2. Structure and difference in rotation

While solving the crystal structure 2 slightly different rotations was found for $FNR1_{mutant}$. The structure named cube shape after the crystal form seen in the microscope was equal to earlier crystallizations of FNR1, while the diamond shape had slight differences. The cube shaped structure has a single dimer as the asymmetric unit, while the diamond shape has 4 dimers as the asymmetric unit. For diamond shape the NADPH-domain has a slight rotation. This rotation makes it different from $FNR1_{mutant}$ and $FNR1_{wild\ type}$, but also does not make the structure more equal to FNR2. As 2 different rotations are found this could either indicate that $FNR1_{mutant}$ is quite prone to rotational changes, or that his329 plays a role in the stability of $FNR1_{mutant}$. For any conclusion to be drawn on this more studies must be performed, as there is not enough data to conclude on cause of difference in rotation.

5 Appendix

5.1. Abbreviations

B. cereus	*Bacillus cereus*
BL21-cells	*E. coli* BL21 (DE3) Competent cells
E. coli	*Escherichia coli*
Fld	Flavodoxin
Fld2	Flavodoxin [BC3541]
FD	Ferredoxin
FMN	Flavin mononucleotide
FAD	Flavin adenine dinucleotide
LB	Luria Broth
$NADP^+$	Nicotinamide adenine dinucleotide phosphate, oxidized
NADPH	Nicotinamide adenine dinucleotide phosphate, reduced
PCR	Polymerase chain reaction
Redox	Reduction-reaction
RNR	Ribonucleotide reductase
SDS-PAGE	Sodium dodecyl sulphate polyacrylamide gel electrophoresis
Native-PAGE	Native polyacrylamide gel electrophoresis
TB	Terrific Broth
UV-vis	Ultraviolet and visible light
FNR	Ferredoxin/flavodoxin NADPH reductase
FNR1	Ferredoxin/flavodoxin NADPH reductase 1 [BC0385]
FNR2	Ferredoxin/flavodoxin NADPH reductase 2 [BC4926]
IEX	Ion Exchange Chromatography
GF	Gel Filtration
SEC	Size Exclusion Chromatography
IPTG	Isopropyl β-D-1-thiogalactopyranoside
OD	Optical density
DTT	Dithiothreitol
EDTA	Ethylenediaminetetraacetic acid
HEPES	4-(2-Hydroxyethyl) piperazine-1-ethanesulfonic acid

5.2. Materials and instruments

Chromatographic Columns

Type of column	Manufacturer
HiTrap Desalting Column	GE Healthcare
HiTrap Q HP Anion Exchange Column	Cyvita
Superdex 200 Increase 10/300 GL Column	GE Healthcare

Hardware

Hardware	Manufacturer
Äkta purifier system	GE Healthcare
Cary 60 UV-vis spectrophotometer	Agilent Technologies
EPS 600 Electrophoresis Power Supply	Pharmacia Biotech
JA-10 rotor	Beckman Coulter
JA-25.50 rotor	Beckman Coulter
Mosquito crystallization robot	SPT Labtech
VC-750 Vibra-Cell Ultrasonic Processor	Sonics & Materials

Equipment

Equipment	Manufacturer
Amicon Ultra Centrifugal Filters	Merck
Cuvettes (quartz)	Hellma

Kits and Commercial crystallization screens

Kit	Manufacturer
NuPAGE Bis-Tris Gels	ThermoFisher
NativeMark Unstained Protein Standard	Invitrogen
Morpheus	Molecular Dimensions
SaltRX	Hampton Research

5.3. Buffers and solutions

LB Medium, 0.5 L

NaCl	5 g
Peptone	5 g
Yeast extract	2.5 g

Dissolved in 0.5 L mqH2O and autoclaved at 121 ºC for 20 min.

When preparing agar for Petri dishes, 10 g agar was added prior to autoclavation.

TB Medium, 12 L

Tryptone	150 g
Yeast extract	300 g
Glycerol	50 ml

Dissolved in 12 L mqH2O and autoclaved at 121 ºC for 20 min.

Buffer A

50 mM Tris

1 mM DTT

2 mM EDTA

pH adjusted to 7.5 by the addition of 12 M HCl

Buffer B

50 mM Tris

1 M KCL

1 mM DTT

2 mM EDTA

pH adjusted to 7.5 by the addition of 12 M HCl

Lysis buffer

100 mM Tris

1 mM DTT

2 mM EDTA

5 ug/mL DNase

pH adjusted to 7.5 by the addition of 12 M HCl

HEPES buffer

50 mM HEPES

100 mM KCl

1 mM DTT

pH adjusted to 7.5 by the addition of 10 M HCl

Fix solution, 100 ml

40 ml Methanol

10 ml Acetic acid

50 ml mqH2O

Destain solution, 100 ml

8 ml Acetic acid

92 ml mqH2O

Crystallization solution - Morpheus

0.1M Carboxylic acid (Molecular Dimensions)

0.1 M Buffer system 2 (Molecular Dimensions)

37.5 % v/v Precipitant mix 4 (Molecular Dimensions)

Crystallization solution - SaltRX

1.5 M lithium sulfate

0.1 M Tris

pH adjusted to 8.5

5.4. Sequences

FNR1$_{\text{wild type}}$ – BC0385

MNREELFDVTVIGGGPAGLYSAFYSGLREMRTKIIEFHPHLGGKIHVYPEKMIWDVG
GLLPVTGDKLIEQLVQQGLTFKPEVVLDTKVESIIRNQDGTFTLKTSTGEEHFSKTVIV
ATGSGILKPQKLSIEGAERFEVSNLNYTVKSLKRFKGKTVIISGGGNSAVDWANELE
PIAKKVYVTYRKEELSGHEAQVKQLMNSSAECFFNTSITKLIAGDNHEAIEYVELTNH
ETGEVSHLPIDEVIINHGYERDITLLENSELDVAIIDNYYIAGNANSESSVDGLYAAGDI
LKHEGKLHLIAGAFQDAGNAVNKAKQFIQPDASEYGMVSSHNEVFKKRNRELIKQM
MK

FNR1$_{\text{mutant}}$

MNREELFDVTVIGGGPAGLYSAFYSGLREMRTKIIEFHPHLGGKIHVYPEKMIWDVG
GLLPVTGDKLIEQLVQQGLTFKPEVVLDTKVESIIRNQDGTFTLKTSTGEEHFSKTVIV
ATGSGILKPQKLSIEGAERFEVSNLNYTVKSLKRFKGKTVIISGGGNSAVDWANELE
PIAKKVYVTYRKEELSGHEAQVKQLMNSSAECFFNTSITKLIAGDNHEAIEYVELTNH
ETGEVSHLPIDEVIINHGYERDITLLENSELDVAIIDNYYIAGNANSESSVDGLYAAGDI
LKHEGKLHLIAGAFQDAGNAVNKAKQFIQPDASEYGMHSSHNEVFKKRNRELIKQM
M

Fld2 – BC3541

MLEGDAKVAKILIAYASMSGNTESIADLIKVSLDAFDHEVVLQEMEGMDAEELLAYD
GIILGSYTWGDGELPFEAEDFHDDLENIDLAGKKVAVFGSGDTAYELFCEAVTIFEEL
VERGAELVQEGLKIELAPEDEEDVEKCSNFAIAFAEKF

NrdI – BC1353

MLVAYDSMTGNVKRFIHKLNMPAVQIDEDLVIDEDFILITYTTGFGNVPERVLDFLER
NNEKLKGVSASGNRNWGDMFGASADKISTKYEVPIVSKFELSGTNNDVEYFKERVR
EIATH

Transformation plasmid

Manufacturer	GenScript
Gene name	BC0385
Vector name	pET-22b(+)

Cloning sites HindIII,NdeI

Codon optimized

Sequence:

ATGAACCGTGAGGAACTGTTCGACGTGACCGTTATCGGTGGCGGT
CCGGCGGGTCTGTACAGCGCGTTCTATAGCGGCCTGCGTGAGATG
CGTACCAAGATCATTGAATTTCACCCGCACCTGGGCGGTAAAATC
CACGTGTACCCGGAGAAAATGATTTGGGACGTGGGCGGTCTGCTG
CCGGTTACCGGTGATAAACTGATCGAACAGCTGGTGCAGCAAGGC
CTGACCTTTAAGCCGGAAGTGGTTCTGGACACCAAAGTTGAAAGC
ATCATTCGTAACCAAGATGGTACCTTCACCCTGAAGACCAGCACC
GGCGAGGAACACTTTAGCAAAACCGTGATCGTTGCGACCGGTAGC
GGCATTCTGAAGCCGCAGAAACTGAGCATCGAGGGTGCGGAACGT
TTCGAAGTGAGCAACCTGAACTATACCGTTAAGAGCCTGAAACGT
TTTAAGGGCAAAACCGTGATCATTAGCGGCGGTGGCAACAGCGCG
GTTGACTGGGCGAACGAGCTGGAACCGATTGCGAAGAAAGTGTAC
GTTACCTATCGTAAAGAGGAGCTGAGCGGTCACGAGGCGCAGGTG
AAACAACTGATGAACAGCAGCGCGGAATGCTTCTTTAACACCAGC
ATCACCAAGCTGATTGCGGGTGATAACCACGAAGCGATCGAGTAC
GTTGAACTGACCAACCACGAGACCGGTGAAGTGAGCCACCTGCCG
ATCGACGAGGTTATCATTAACCACGGCTATGAACGTGATATTACC
CTGCTGGAGAACAGCGAACTGGACGTGGCGATCATTGATAACTAC
TATATTGCGGGTAACGCGAACAGCGAGAGCAGCGTTGACGGTCTG
TACGCGGCGGGTGATATCCTGAAGCACGAAGGCAAACTGCACCTG
ATTGCGGGTGCGTTCCAGGACGCGGGTAACGCGGTTAACAAGGCG
AAACAGTTTATCCAACCGGATGCGAGCGAGTATGGTATGGTTAGC
AGCCACAACGAGGTTTTCAAGAAACGTAACCGTGAACTGATTAAG
CAAATGATGAAATAA

6 Reference list

1. Weber, S. and E. Schleicher, *Flavins and Flavoproteins : Methods and Protocols*. 2014, Springer New York : Imprint: Humana: New York, NY.
2. Chaiyen, P. and N.S. Scrutton, *Special Issue: Flavins and Flavoproteins: Introduction.* FEBS J., 2015. **282**(16): p. 3001-3002.
3. Lackie, J.M., *Flavoproteins*, in *A dictionary of Biomedicine*. 2013, Oxford University Press. p. 243-243.
4. Sancho, J., *Flavodoxins: sequence, folding, binding, function and beyond.* Cell Mol. Life Sci., 2006. **63**(7): p. 855-864.
5. Kimata-Ariga, Y., Y. Chikuma, T. Saitoh, M. Miyata, Y. Yanagihara, K. Yamane, and T. Hase, *NADP(H) allosterically regulates the interaction between ferredoxin and ferredoxin-NADP+ reductase.* FEBS Open Bio, 2019. **9**(12): p. 2126-2136.
6. Gudim, I., M. Hammerstad, M. Lofstad, and H.-P. Hersleth, *The Characterization of Different Flavodoxin Reductase-Flavodoxin (FNR-Fld) Interactions Reveals an Efficient FNR-Fld Redox Pair and Identifies a Novel FNR Subclass.* Biochemistry, 2018. **57**(37): p. 5427-5436.
7. Aliverti, A., V. Pandini, A. Pennati, M. de Rosa, and G. Zanetti, *Structural and functional diversity of ferredoxin-NADP+ reductases.* Arch. Biochem. Biophys., 2008. **474**(2): p. 283-291.
8. Teufel, R., V. Agarwal, and B.S. Moore, *Unusual flavoenzyme catalysis in marine bacteria.* Curr. Opin. Chem. Biol., 2016. **31**: p. 31-39.
9. Macheroux, P., B. Kappes, and S.E. Ealick, *Flavogenomics – a genomic and structural view of flavin-dependent proteins.* FEBS J., 2011. **278**(15): p. 2625-2634.
10. Christopher, C.M., P.P. Satya, M.s. Pavel, and M. Bettie Sue, *Diminished FAD Binding in the Y459H and V492E Antley-Bixler Syndrome Mutants of Human Cytochrome P450 Reductase.* J. Biol. Chem., 2006. **281**(47): p. 35975-35982.
11. Chapman, S.K. and G.A. Reid, *Flavoprotein Protocols*. 1999, Humana Press : Imprint: Humana: Totowa, NJ.
12. Skråmo, S., H.P. Hersleth, M. Hammerstad, K.K. Andersson, and Å.K. Røhr, *Cloning, expression, purification, crystallization and preliminary X-ray diffraction analysis of a ferredoxin/flavodoxin-NADP(H) oxidoreductase (Bc0385) from Bacillus cereus.* Acta Cryst. F Struct. Biol. Commun., 2014. **70**(6): p. 777-780.
13. Muraki, N., D. Seo, T. Shiba, T. Sakurai, and G. Kurisu, *Asymmetric Dimeric Structure of Ferredoxin-NAD(P)+ Oxidoreductase from the Green Sulfur Bacterium Chlorobaculum tepidum: Implications for Binding Ferredoxin and NADP.* J. Mol. Biol., 2010. **401**(3): p. 403-414.
14. Seo, D., T. Asano, H. Komori, and T. Sakurai, *Role of the C-terminal extension stacked on the re-face of the isoalloxazine ring moiety of the flavin adenine dinucleotide prosthetic group in ferredoxin-NADP+ oxidoreductase from Bacillus subtilis.* Plant. Physiol. Biochem., 2014. **81**: p. 143-148.
15. Komori, H., D. Seo, T. Sakurai, and Y. Higuchi, *Crystal structure analysis of Bacillus subtilis ferredoxin-NADP+ oxidoreductase and the structural basis for its substrate selectivity.* Protein Sci., 2010. **19**(12): p. 2279-2290.
16. Karabencheva-Christova, T., *Dynamics of Proteins and Nucleic Acids*. Advances in protein chemistry and structural biology. Vol. ninety two. 2013, San Diego: San Diego: Elsevier Science & Technology.
17. Torrents, E., *Ribonucleotide reductases: essential enzymes for bacterial life.* Front. Cell. Infect. Microbiol., 2014. **4**: p. 52-52.

18. Stubbe, J. and M.R. Seyedsayamdost, *Discovery of a New Class I Ribonucleotide Reductase with an Essential DOPA Radical and NO Metal as an Initiator of Long-Range Radical Transfer*. Biochemistry, 2019. **58**(6): p. 435-437.
19. Lofstad, M., I. Gudim, M. Hammerstad, Å.K. Røhr, and H.-P. Hersleth, *Activation of the Class Ib Ribonucleotide Reductase by a Flavodoxin Reductase in Bacillus cereus.* Biochemistry, 2016. **55**(36): p. 4998-5001.
20. Brown, T.A., *Gene Cloning and DNA Analysis: An Introduction*. 2016, Somerset: Somerset: John Wiley & Sons, Incorporated.
21. Johnston, C., B. Martin, G. Fichant, P. Polard, and J.-P. Claverys, *Bacterial transformation: distribution, shared mechanisms and divergent control.* Nat. Rev. Microbiol., 2014. **12**(3): p. 181-196.
22. Voet, D. and J.G. Voet, *Biochemistry*. 3rd ed. ed. 2004, Hoboken: Wiley.
23. Berg, J.M., L. Stryer, J.L. Tymoczko, and G.J. Gatto, *Biochemistry*. Ninth edition. ed. 2019, New York: Macmillan Learning.
24. JoVE Science Education Database. Basic Methods in Cellular and Molecular Biology. *Separating Protein with SDS-PAGE, 2021*. MyJoVE Corp.
25. McPherson, A. and J.A. Gavira, *Introduction to protein crystallization.* Acta Cryst. F Struct. Biol. Commun., 2014. **70**(1): p. 2-20.
26. *SaltRx* , H. Research, Editor. 2019: https://hamptonresearch.com/uploads/support_materials/HR2-136_binder.pdf.
27. Gorrec, F., *The MORPHEUS protein crystallization screen.* J. Appl. Cryst., 2009. **42**(6): p. 1035-1042.
28. Vonrhein, C., C. Flensburg, P. Keller, A. Sharff, O. Smart, W. Paciorek, T. Womack, and G. Bricogne, *Data processing and analysis with the autoPROC toolbox.* Acta Cryst. D, 2011. **67**(4): p. 293-302.
29. Kabsch, W., *XDS.* Acta Cryst. D, 2010. **66**(2): p. 125-132.
30. Winn, M.D., C.C. Ballard, K.D. Cowtan, E.J. Dodson, P. Emsley, P.R. Evans, R.M. Keegan, E.B. Krissinel, A.G.W. Leslie, A. McCoy, S.J. McNicholas, G.N. Murshudov, N.S. Pannu, E.A. Potterton, H.R. Powell, R.J. Read, A. Vagin, and K.S. Wilson, *Overview of the CCP4 suite and current developments.* Acta Cryst. D, 2011. **67**(4): p. 235-242.
31. Emsley, P., B. Lohkamp, W.G. Scott, and K. Cowtan, *Features and development of Coot.* Acta Cryst. D, 2010. **66**(4): p. 486-501.
32. Evans, P.R. and G.N. Murshudov, *How good are my data and what is the resolution?* Acta Cryst. D, 2013. **69**(7): p. 1204-1214.
33. McCoy, A.J., R.W. Grosse-Kunstleve, P.D. Adams, M.D. Winn, L.C. Storoni, and R.J. Read, *Phaser crystallographic software.* J. Appl. Cryst, 2007. **40**(4): p. 658-674.
34. Murshudov, G.N., P. Skubák, A.A. Lebedev, N.S. Pannu, R.A. Steiner, R.A. Nicholls, M.D. Winn, F. Long, and A.A. Vagin, *REFMAC5 for the refinement of macromolecular crystal structures.* Acta Cryst. D, 2011. **67**(4): p. 355-367.
35. Kobylarz, M.J., G.A. Heieis, S.A. Loutet, and M.E.P. Murphy, *Iron Uptake Oxidoreductase (IruO) Uses a Flavin Adenine Dinucleotide Semiquinone Intermediate for Iron-Siderophore Reduction.* ACS Chem. Biol., 2017. **12**(7): p. 1778-1786.